Artemisinin-Derivative-NHC-gold(I)-Hybrid with enhanced cytotoxic activity through inhibiting NRF2 transcriptional activity

Chen Zhang, Pierre-Yves Fortin, Guillaume Barnoin, Xue Qin, Xing Wang, Alvaro Fernandez Alvarez, Christian Bijani, Marie-Lise Maddelein, Catherine Hemmert, Olivier Cuvillier, et al.

Artemisinin-Derivative-NHC-gold(I)-Hybrid with enhanced cytotoxic activity through inhibiting NRF2 transcriptional activity

Chen Zhang[1,2,$], Pierre-Yves Fortin[2,$], Guillaume Barnoin[1,$], Xue Qin[1], Xing Wang[1], Alvaro Fernandez Alvarez[1], Christian Bijani[1], Marie-Lise Maddelein[2], Catherine Hemmert[1,*], Olivier Cuvillier[2,*], Heinz Gornitzka[1,*]

[1] LCC-CNRS, Université de Toulouse, CNRS, UPS, Toulouse, France

E-mail: hemmert@lcc-toulouse.fr and gornitzka@lcc-toulouse.fr

[2] Institut de Pharmacologie et de Biologie Structurale, Université de Toulouse, CNRS, UPS, Toulouse , France

E-mail: olivier.cuvillier@inserm.fr

[$] These authors contributed equally to this work.

Supporting information for this article is given via a link at the end of the document.

Abstract

A family of original bis(artemisinin-NHC)gold(I) complexes have been synthesized. These hybrid molecules combine two biological active motifs, an artemisinin derivative (DHA) and a cationic bis(NHC)gold(I) unit. One of these complexes, complex **2a**, has been analyzed by single-crystal X-ray diffraction and tested in depth for its anticancer properties. Complex **2a** shows strong anticancer activities on a representative panel of human cancer cell models from 8 different localizations (prostate, breast, lung, liver, bladder, bone, acute and chronic myeloid leukemias). Complex **2a** shows anticancer activity to a much better degree than Auranofin and DHA standards with GI_{50} values in nM range, together with a superior

selectivity in regard to non-cancer cell models. Next to expected ROS formation and TrxR inhibition, an original and distinctive mechanism of action through inhibition of NRF2 — a transcription factor strongly associated with aggressiveness and resistance to cancer therapies — with an IC_{50} value at nM range has been evidenced. Importantly, the NRF2 inhibitory effect of complex **2a** could remarkably sensitize to sorafenib in HepG2 liver cells, in which dysregulated NRF2 signaling is known to be associated with primary and acquired drug resistance. Moreover, complex **2a** also inhibited NF-κB and HIF transcriptional activities, which are also linked to progression and resistance in cancer. Our findings provide experimental evidence that hybrid (NHC)gold(I) molecules —such as complex **2a** — represent a new class of organometallic hybrid molecules that may yield new therapeutic agents.

Keywords: Metallodrugs, Gold, Artemisinin, Chemoresistance, Cancer, NRF2, NF-κB, HIF, Sorafenib, Hypoxia

Introduction

Artemisinin and its derivatives represent the most important class of drugs to combat malaria nowadays. During the period from 2010 to 2017 the number of deaths worldwide caused by malaria decreased by 28% mainly due to the use of artemisinin-based combination therapies [1]. Nevertheless, the interests on artemisinin derivatives is not only focused on malaria, it has been shown that these compounds show interesting activities against viral diseases and cancer [2, 3, 4, 5]. In the context of cancer, one mechanism of action is based on ROS formation, due to an activation of artemisinin derivatives by iron from free heme [5, 6, 7, 8]. This activation takes mainly place in mitochondria, where fresh heme is produced continuously. It has been evidenced that mitochondria-targeting artemisinin derivatives show stronger anticancer activities than non-mitochondria-targeting ones [6]. Another class of molecules, cationic *N*-heterocyclic carbene (NHC) gold(I) complexes show also solid anticancer activities and the main mechanism of action discussed concerns apoptosis due to an antimitochondrial activity of such complexes [9, 10, 11, 12]. During the last few years we focused our research on the optimization of NHC gold(I) complexes for anticancer activities [13, 14, 15]. Herein we present the synthesis, cytotoxic, selectivity and mechanistic studies of cationic bisNHC gold(I) complexes incorporating an ether derivative of dihydroartemisinin (DHA, semi-synthetic derivative of artemisinin and metabolite of all artemisinin compounds) as building block.

Results

In order to fuse DHA and NHCs precursors we used aliphatic linkers of different lengths C3 to C5. The synthesis (Figure 1) starts with the formation of an ether, by reacting commercially DHA with a bromoalcohol in the presence of boron trifluoride etherate catalyst according to the procedure described by Haynes for the C3-derivative, leading to the single β-isomers DHA-C3 to DHA-C5 [16]. The next step was the reaction between the bromoalkyl DHA derivatives and methyl imidazole in order to obtain the corresponding carbene precursors **1a** to **1c** with yields ranging from 39 to 92%. The formation of the target gold complexes has been achieved by two approaches. For the C3 derivative, the convenient transmetalation route involving the mild base Ag_2O, followed by an ion exchange with $AgNO_3$ and subsequent addition of $Au(SMe_2)Cl$ has been used. For the C4 and C5 derivatives, the direct metalation involving K_2CO_3 and $Au(SMe_2)Cl$ has been applied. The gold(I) complexes **2a-c** were isolated after purification by chromatography as white solids with yields of 31 to 84%. All compounds were characterized by ^{1}H and ^{13}C NMR spectroscopy, high-resolution mass spectrometry and elemental analysis (see the Supporting Information). ^{13}C NMR spectroscopy unequivocally evidences the formation of the cationic gold(I) complexes with resonance of the carbenic carbons located at 183.6-183.7 ppm. HRMS spectra of **2a-c** exhibit the classical peak for the cationic fragment $[M - X^-]^+$ and elemental analysis correspond to the general $[AuL_2][X]$ formula. Moreover, single crystals suitable for X-ray structure analysis have been obtained by gas phase diffusion from diethyl ether to a saturated solution of **2a** in acetonitrile (Figure 1). In the solid state the gold(I) shows the typical linear coordination stabilized by two NHC ligands. The NHC planes are crossed around the C-Au-C axis with torsion angles from 116° to 138°. It is remarkable that

the bulky DHA-derivative groups are on the same side of the central bisNHC gold motif. This is due to an aurophilic interaction leading to a dimeric form in the solid state of the complex with Au-Au distance of 345.0 pm.

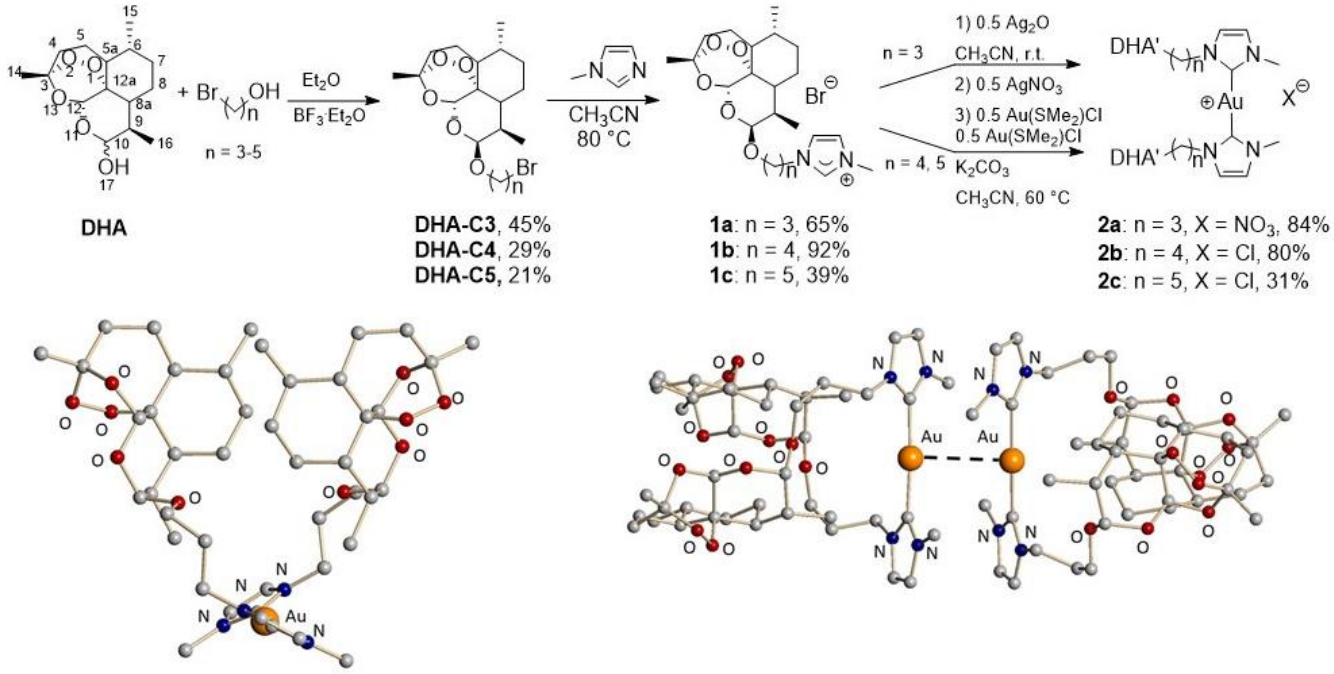

Figure 1. On the top: synthesis of proligands **1a-c** and gold(I) complexes **2a-c**. On the bottom is depicted the structure of the cationic part of **2a** in the solid state. One bisNHC gold unit looking along the C-Au-C axis on the left and dimeric arrangement on the right.

In a first anticancer screening, precursors **1a-c** and complexes **2a-c** were evaluated for their *in vitro* cytotoxic abilities against the PC-3 prostate cancer cell line and two non-cancer cell lines (NIH3T3 fibroblastic and RPWE-1 epithelial prostatic cell lines) (Table 1). Interestingly, the imidazolium salts **1a-c** showed no cytotoxic effects (GI_{50} > 20 µM), while complexes **2a-c** exhibited strong antiproliferative activities with GI_{50} values between 20 nM and 70 nM. The selectivity indexes (SI = GI_{50} (non-cancer cell line) / GI_{50} (cancer cell line)) of **2a-c** gave nearly the same values concerning NIH3T3 cells ranging from 15.5 to 16.7, while RPWE-1 cells gave a more differentiated result with the highest SI = 6.9 for **2a**.

Table 1. Cytotoxicity and selectivity of compounds **1a-c** and **2a-c** on PC-3 prostate cancer cells versus non tumoral NIH3T3 mouse embryonic fibroblasts and RWPE-1 human prostatic epithelial cells (GI_{50} [μM], 72 h, MTT assay).[a]

	PC-3	NIH3T3	SI[b]	RWPE-1	SI[b]
1a	> 20	> 20	-	> 20	-
1b	> 20	> 20	-	> 20	-
1c	> 20	> 20	-	3.74	-
2a	0.070	1.13	16.2	0.480	6.9
2b	0.042	0.700	16.7	0.110	2.6
2c	0.020	0.310	15.5	0.098	4.9
Auranofin	1.09	1.10	1.0	0.084	0.1
DHA	1.56	3.86	2.5	9.68	6.5
3	0.695	7.98	11.8	0.112	0.1
3 / DHA (1:2)	1.09	2.85	2.6	0.218	0.2

[a] The GI_{50} values represent the concentration of compound causing 50% inhibition of cell growth. Mean of at least three independent experiments.
[b] Selectivity index ((SI = GI_{50} (non-cancer cell line) / GI_{50} (cancer cell line)).

As reference drugs for our studies, along with DHA, we tested the gold complex auranofin, used for treating inflammatory arthritis, and now proposed for drug repurposing in cancer [17], which recently entered phase I/II trials in lung cancer in combination with mTOR inhibitor sirolimus (Clinicaltrials.gov ID NCT01737502). Moreover, a published cationic bisNHC gold(I) complex **3**, containing a methyl and a quinoline substituents [18], and a mixture of **3** and DHA (1:2) were investigated in order to evaluate the potential synergism effect of the hybrid complexes. Outstandingly, complexes **2a-c** displayed 16 to 55-fold and 22 to 78-fold higher potency than auranofin and DHA on PC-3 cells, respectively. Moreover, they were 6.2 to 16.7 more selective towards cancer cells than NIH3T3 compared to the two drug references. Remarkably, complex **2a** shows a PC-3/RPWE-1 SI value close to that of

DHA but 69 times higher than that obtained for both gold references, auranofin and complex **3**. Complex **3** showed 10 to 35-fold lower activity than **2a-c** and the mixture of **3** and DHA has an efficiency between DHA and **3** with a low selectivity. Overall, these results highlight that linking a derivative of DHA on the NHC scaffold of a bisNHC gold(I) unit results in an effect characterized by a high cytotoxicity combined with a high selectivity.

Due to its better selectivity, complex **2a** was chosen for further biological investigations. Besides PC-3 prostate cancer, **2a** was thus tested on a panel of seven other representative human cancer cell models, namely A549 (lung), U-2 OS (bone), MCF-7 (breast), T24 (bladder), LAMA (chronic myeloid leukemia), HL-60 (acute myeloid leukemia) and HepG2 (liver). An additional noncancerous cell line, the MC3T3 pre-osteoblastic cell line was also tested (Table 2).

Table 2. Cytotoxicity of complex **2a**, auranofin, DHA, complex **3** and a mixture of complex **3** and DHA (1:2 ratio) on a representative panel of cancer cell lineages and the non tumoral MC3T3 mouse osteoblastic cell line (GI_{50} [µM], 72 h, MTT assay).[a]

	A549 Lung	U-2 OS Bone	MCF-7 Breast	T24 Bladder	LAMA CML	HL-60 AML	HepG2 Liver	MC3T3 Bone
2a	0.115	0.122	0.089	0.175	0.079	0.017	2.43	1.62
Auranofin	4.41	0.474	1.39	1.10	0.809	0.951	3.62	1.39
DHA	11.1	4.10	9.67	4.99	5.60	3.25	12.0	3.55
3	1.16	2.51	0.380	0.191	0.662	0.500	5.23	17.9
3 / DHA (1:2)	1.99	1.25	0.610	0.319	0.800	0.471	4.71	1.76

[a] The GI_{50} values represent the concentration of compound causing 50% inhibition of cell growth. Mean of at least three independent experiments.

As in the case of PC-3 cells the GI_{50} values for six cancer cell lines were in the lower nM range spanning from 79 to 175 nM. Overall, complex **2a** exhibited a much stronger

potency than auranofin (15-fold), DHA (60-fold), complex **3** (9-fold) and the mixture of **3** and DHA (10-fold) in the representative prostate, lung, bone, breast, bladder and leukemia cells. Of note, **2a** was 13.3 times more selective towards U-2 OS bone cancer cells than MC3T3 normal bone cells, much higher than auranofin (2.9-fold), whereas DHA did not express any selectivity. The efficacy of complex **2a** was confirmed using a clonogenic assay (or colony formation assay), an *in vitro* cell survival assay based on the ability of a single cell to form a colony (>50 cells), and a method of choice to determine the effectiveness of radiotherapy or cytotoxic agents [19]. At concentrations above 100 nM, no visible colony of PC-3 prostate or T24 bladder cells could be observed, indicating the ability of low concentrations complex **2a** to completely abolish the capacity of these cells to proliferate (Suppl. Fig 1).

Overall, these results show that hybrid complex **2a** is extensively more effective than the control molecules used in this study on all the tested cancer cell line models, even on hepatocellular carcinoma HepG2, a cancer model notoriously known to be difficult to treat by chemotherapy [20], suggesting that gold(I)-artemisinin like hybrid complexes could represent potential novel anticancer drugs.

High reactive oxygen species (ROS) levels are harmful to cells, and oxidative stress can have a tumor-suppressive effect [21]. ROS levels were increased after treatment with auranofin or complex **2a**, and a weaker effect on ROS formation was noted for DHA in some cell lines (Suppl. Fig 2). In general, no significant differences in the amount of generated ROS were observed across cell lines and treatments, suggesting that the amount of ROS produced could not explain the differential anti-tumor efficacies among treatments. The

behavior of cell lines to ROS-mediated cell death is strongly dependent on antioxidant enzymes or oxidative stress regulators. In this respect, the NRF2 antioxidant response pathway plays a fundamental role to protect our body against drug toxicity and stress-induced diseases, by notably regulating the basal and inducible expression of detoxification and antioxidant enzymes [22]. Although NRF2 activation is normally beneficial for health, persistent NRF2 activation has undesirable effects in cancer, promoting malignant progression by conferring chemo-and radioresistance, as well as promoting metabolic reprogramming [22]. To quantify NRF2 antioxidant response activity, we relied on an ARE Reporter – HepG2 liver cancer cell model containing a firefly luciferase gene under the control of a stably integrated ARE (antioxidant response element). Tert-butylhydroquinone or tBHQ was used to validate the response to stimulation of the ARE Reporter – HepG2 cell line (Fig 2a). Both auranofin and DHA (and its bioactive derivatives) have been extensively reported to stimulate NRF2 transcriptional activity in various physio(patho)logical conditions including in cancer [23, 24, 25, 26, 27]. Indeed, the treatment with auranofin (Fig 2b) or DHA (Fig 2c) markedly increased NRF2 transcriptional activity. To the best of our knowledge ARE activity monitoring has never been reported with cationic bisNHC gold(I) complexes such as complex **3**. In contrast to auranofin and DHA, complex **3** treatment was associated with a stimulation of ARE activity mostly significant beyond 1 μM (Fig 2d). Unexpectedly, owing to the fact that both DHA and complex **3** stimulated ARE activity in HepG2 cell line, the hybrid complex **2a** did not stimulate ARE activity. Instead, the treatment with complex **2a** was associated with a remarkable dose-dependent inhibition of NRF2 transcriptional activity starting as low as 10 nM dose (Fig 2e), and a calculated IC_{50} of 850 nM. To substantiate this finding, we also monitored NRF2 transcriptional activity, by

using an inducible ARE Reporter containing a renilla luciferase gene in a second model, the MCF7 breast cancer cells. As shown in Fig 2f, complex **2a** was again able to inhibit NRF2 transcriptional activity induced by 10 µM of tBHQ (calculated IC_{50} of 1.14 µM) whereas neither auranofin, DHA nor complex **3** were capable of suppressing tBHQ-induced NRF2 activity (data not shown).

Figure 2. Complex **2a** inhibits NRF2 transcriptional activity.
a-e, NRF2 transcriptional activity was evaluated in HepG2 cancer cell model treated with tBHQ, auranofin, DHA, **3** and **2a** compounds. The ARE Reporter – HepG2 cell line contains a firefly luciferase gene under the control of ARE stably integrated into HepG2 cells. This cell line is validated for the response to the stimulation of tert-butylhydroquinone (tBHQ). **f**, the inhibitory effect of complex **2a** was evaluated in NRF2 ARE – Responsive Renilla Reporter MCF-7 human breast cancer, stimulated by 10 µM tBHQ for 7h. Mean of at least three independent experiments ± SD.

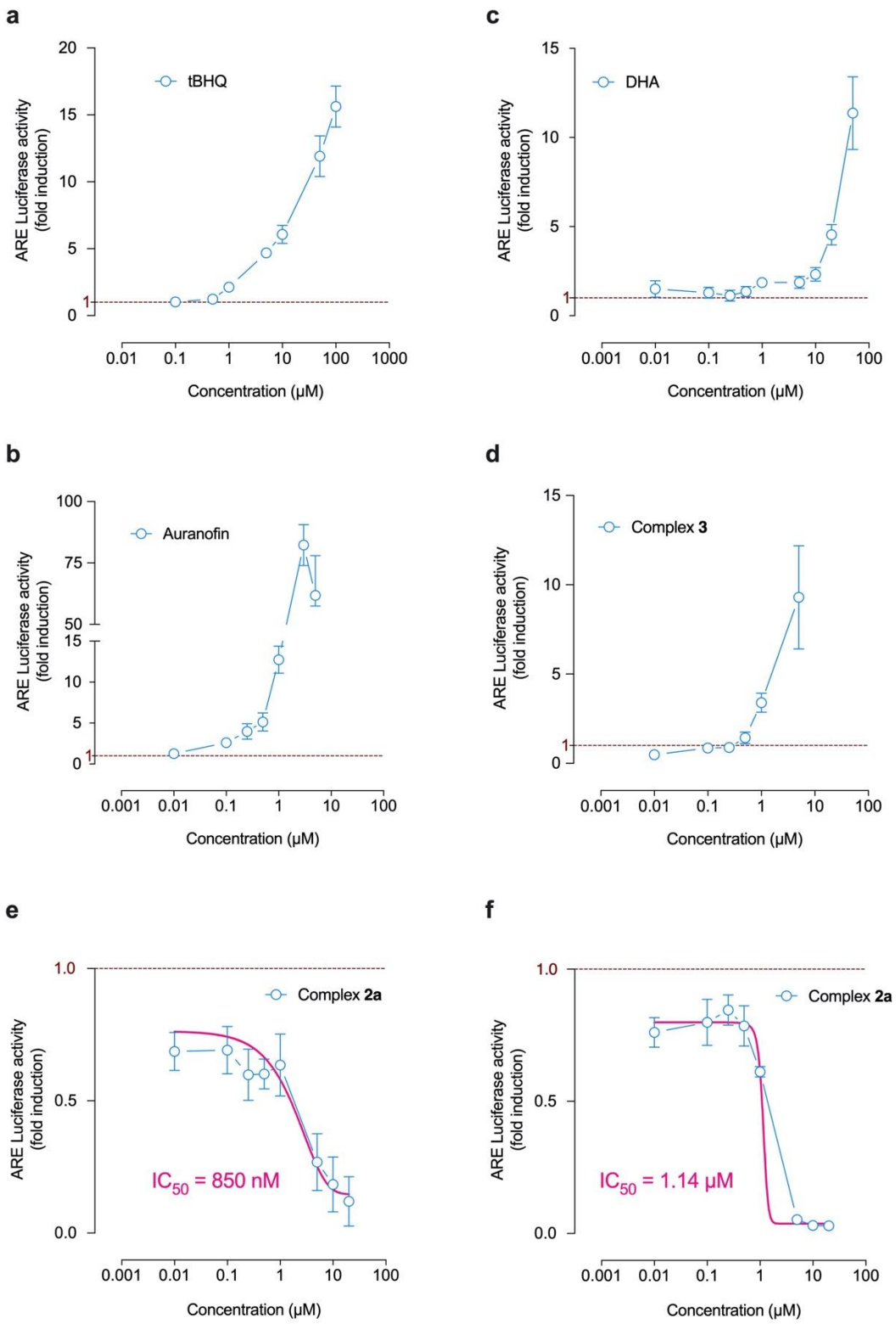
a
tBHQ
ARE Luciferase activity (fold induction)
Concentration (μM)
b
Auranofin
c
DHA
d
Complex 3
e
Complex 2a
IC50 = 850 nM
f
Complex 2a
IC50 = 1.14 μM

Interestingly, NRF2 directly regulates the ATP-binding cassette (ABC) superfamily multidrug efflux pumps expression in a number of human tumors [28]. Overexpression of such multidrug-resistance-associated proteins including MRP1 or MDR1 is recognized as a major impediment to successful chemotherapies *in vitro* and *in vivo* [29]. To further substantiate a role for complex **2a** as a potential anticancer drug, we evaluated its efficacy towards multidrug-resistant HL-60 acute myeloid leukemia cells [30], grown in medium supplemented with increasing concentrations of doxorubicin or etoposide, causing the overexpression of MRP1 or MDR1, respectively [31]. Contrary to parental HL-60 cells (Fig 3a), both doxorubicin and etoposide failed to trigger cell death in chemoresistant HL-60/Doxo (Fig 3b) and HL-60/VP16 cells (Fig 3c). Noteworthy, complex **2a** could overcome resistance to doxorubicin and etoposide in both HL-60/Doxo (Fig 3b) and HL-60/VP16 cells (Fig 3c), with GI_{50} values similar to the one calculated for the chemosensitive parental HL-60 cells. In line with previous reports showing that NRF2 genetic silencing could restore chemosensitivity through a significant downregulation of NRF2-targeted ATP-binding cassette (ABC) efflux transporters, our data suggest that complex **2a** could overcome multidrug-associated chemoresistance.

Figure 3. Complex **2a** overcomes chemoresistance in HL-60 acute myeloid leukemia.
Parental HL-60 cells (**a**), HL-60/Doxo (**b**) and HL-60/VP16 (**c**) were incubated in the absence or presence of 1 mM doxorubicin or 5mM etoposide (VP16) or with increasing concentration of complex **2a** for 72h. (GI_{50} [µM], 72 h, MTT assay).[a] Mean of at least three independent experiments ± SD.

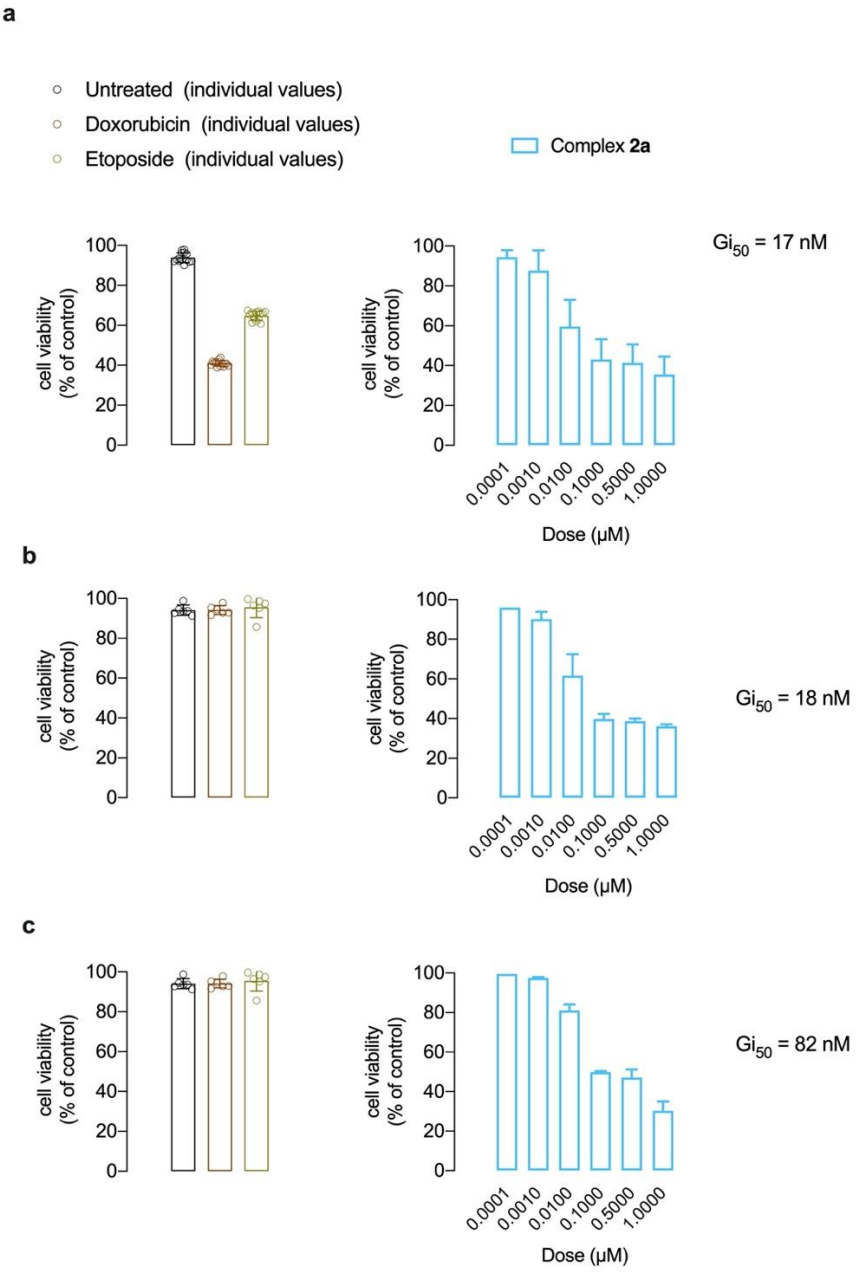

We next attempted to study the potential chemosensitizing effects of complex **2a** particularly in liver cancer, where the multiple kinase inhibitor sorafenib is the first-line systemic therapy since 2007. Yet, sorafenib has been shown to provide limited survival benefits, suggesting the existence of primary and acquired drug resistance mechanisms, and several lines of evidence suggest a key role for NRF2 signaling. First, somatic mutations of

NRF2 and Keap1 — the repressor protein that binds to NRF2 and promotes its degradation by the ubiquitin proteasome pathway — have been documented in hepatocarcinoma [32]. Second, exome analyses have shown that NRF2 is a driver gene for liver carcinogenesis [33]. Third, sorafenib itself can augment both mRNA and protein levels of NRF2 in hepatocarcinoma [34, 35]. In that regard, Sun and co-workers recently demonstrated that shRNA strategy against NRF2 was able to significantly enhance the anticancer activity of sorafenib in hepatocarcinoma cell and animal models [34]. Accordingly, we hypothesized that the NRF2 inhibitory effect of complex **2a** could sensitize to sorafenib in HepG2 cells. The treatment of HepG2 cells with sorafenib was indeed associated with a significant increase in NRF2 transcriptional activity (Fig 4a). As anticipated, complex **2a** remarkably reversed the NRF2 transcriptional activity surge induced sorafenib, starting as low as 10 nM dose, with a calculated IC_{50} of 511 nM (Fig 4b). To establish the proof-of-concept that complex **2a** could therefore serve as a sensitizing agent for sorafenib in hepatocarcinoma, we relied on an isobologram analysis [36]. Complex **2a** displayed a GI_{50} value of 2.4 μM toward HepG2 (Table 2) whereas the GI_{50} of sorafenib value was achieved at 4.1 μM (data not shown). We exposed HepG2 cells to fixed doses of sorafenib (1 and 2.5 μM) in combination with several doses of complex **2a** ranging from 1 nM to 1 μM, or to fixed doses of complex **2a** (500 nM and 1 μM) combined with 10 nM to 5 μM sorafenib (Fig 4c).

In all tested combinations, the synergy of effect was remarkable with calculated combination indexes (CI) significantly below the value of 1 that represents an additive effect (Fig 4c). Of note, as shown by the CI values (Fig 4c) and the isoboles (Fig 4d), a better synergism was observed with fixed concentration complex **2a** clearly indicating that

inhibition of NRF2 activity by complex **2a** counteracts a mechanism of resistance hereby sensitizing hepatocarcinoma cells to sorafenib.

Figure 4. Complex **2a** sensitizes to sorafenib in HepG2 cells through inhibition of NRF2 activity.
a, NRF2 transcriptional activity was evaluated in HepG2 cancer cell model treated with 1 μM of sorafenib for 7h. The ARE Reporter – HepG2 cell line contains a firefly luciferase gene under the control of ARE stably integrated into HepG2 cells.
b, the inhibitory effect of **2a** compound was evaluated ARE Reporter – HepG2 cell line treated with 1 μM of sorafenib for 7h.
c, Combination Index (CI) of **2a** and sorefenib on HepG2 liver cancer cells (GI_{50} [μM], 72 h, MTT assay).
d, Isobologram for GI_{50} values in which the dose of **2a** alone is 2.43 μM and Sorafenib alone is 4.11 μM. The straight line connecting these intercept points (additivity line) is the locus of all dose pairs that, based on these potencies, should give the same effect. All tested dose pairs attain this effect with lesser quantities and are superadditive or synergistic.

a

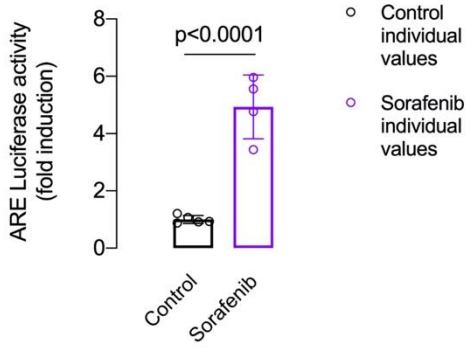

b

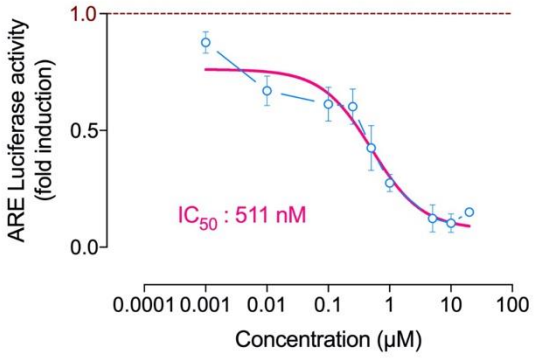

c

Combination of a [fixed concentration of **2a**] and variable concentration of Sorafenib			Combination of a [fixed concentration of Sorafenib] and variable concentration of **2a**		
2a	Sorafenib	**CI** [b]	Sorafenib	**2a**	**CI** [b]
0.500	0.533 [a]	**0.33**	1.000	0.784 [a]	**0.57**
1.000	0.100 [a]	**0.41**	2.500	0.400 [a]	**0.77**

[a] The GI_{50} values represent the concentration of compound causing 50% inhibition of cell growth. Mean of three independent experiments.

[b] CI > 1 means antagonism, CI = 1 means additive effect, CI <1 meany synergy of effect

d

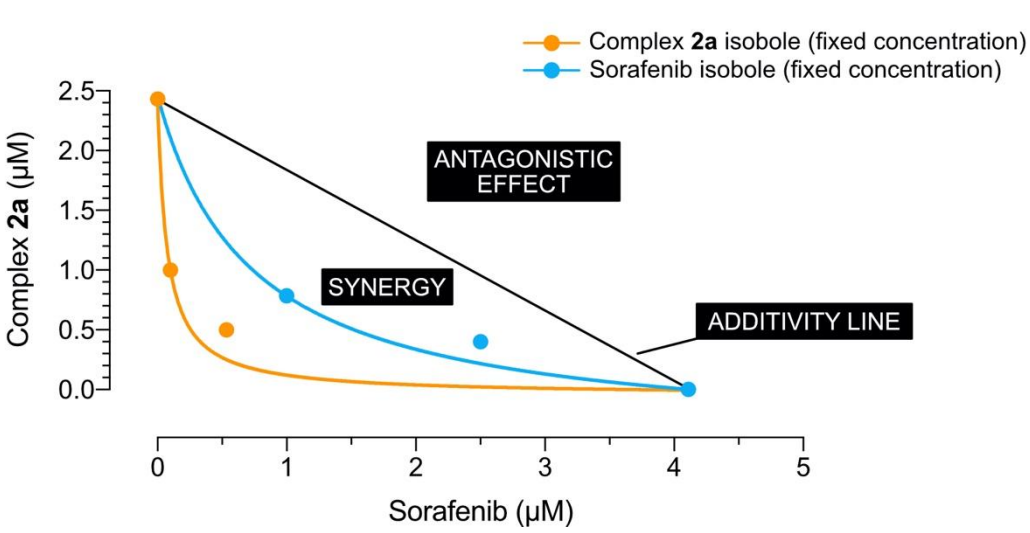

Besides NRF2, two other major transcription factors have been reported to be modulated by arteminsin (and derivatives) or gold-containing drugs, namely NF-κB and Hypoxia Inducible Factor (HIF). The NF-κB signaling cascade mediates pleiotropic functions in the innate and adaptive immune responses. Beyond inflammation, the NF-κB pathway is also involved extensively in cancer development and progression [37, 38, 39]. We made use of a A549 lung cancer cell model in which NF-κB luciferase reporter construct is stably integrated to quantify NF-κB activity. Stimulation of NF-κB was conducted with the TNFα cytokine, and peaked after 7 hours of treatment (Suppl. Fig 3a). Auranofin has been previously reported to inhibit NF-κB activation regardless of the nature of the stimulus (TNFα, IL-1β, LPS) in various cell systems, including cancer [40, 41, 42]. A wealth of reports also establish that artemisinin derivatives inhibit NF-κB activation in numerous solid cancer and hematological cell lineages [43, 44, 45, 46]. Both auranofin and DHA inhibited NF-κB activity triggered by TNFα (Suppl. Fig 3b) with IC_{50} values reminiscent of their capability to inhibit cell proliferation (Table 2). As shown in Suppl. Fig 3b, complex **2a** remarkably suppressed NF-κB activity at very low concentrations (IC_{50} = 627 nM). The inhibitory effect of complex **2a** might be related to the cationic bisNHC gold(I) moiety, also present in complex **3**, which exhibited similar efficacy towards NF-κB activity (IC_{50} = 664 nM, Suppl. Fig 3b). Hypoxia, the decrease in the physiological level of tissue oxygen, is a hallmark of solid tumors, and the adjustment of tumor cells to the lack of oxygen is critical for the development of aggressive tumor phenotype [47] and associated with treatment resistance and poor clinical prognosis [48]. Recent studies have shown that auranofin could sensitize hypoxic tumor cells to irradiation [49], and inhibits NF-κB activation induced by hypoxia [42]. A single direct evidence recently showed that auranofin could inhibit the accumulation of HIF-1α, the

master transcription factor that regulates response to hypoxia [50]. The HRE-Luc Reporter Cell Line-HeLa stably expressing luciferase reporter gene under the control of the hypoxia response element (HRE) was employed to study the hypoxia signaling pathway. In line with the aforementioned studies, HRE-mediated transcription was remarkably decreased by auranofin treatment in HeLa cells (Suppl. Fig 3c) with an IC_{50} of 745 nM. DHA also inhibited HIF activity to a lesser extent similar to its effect on NF-κB activity (IC_{50} > 10 μM). This is in line with a number of studies establishing the anti-hypoxic and subsequent anti-angiogenesis effects of artemisinin and derivatives in cancer cells [51, 52, 53]. The effect of cationic bisNHC gold(I) on HIF activity has never been reported prior this study. As shown in Suppl. Fig 3c, complex **3** also inhibited HIF activity (IC_{50} = 2.0 μM). In keeping with its remarkable effect on NRF2 and NF-κB transcriptional activities, complex **2a** strongly impeded HRE-mediated transcription under hypoxia in HeLa cells with and IC_{50} of 942 nM (Suppl. Fig 3c).

Conclusion

Herein, we report the synthesis, cytotoxicity, selectivity and the biological mechanistical aspects of cationic bisNHC gold(I) complexes incorporating an ether derivative of dihydroartemisinin (DHA, semi-synthetic derivative of artemisinin and metabolite of all artemisinin compounds) as building block. Hybride-complex **2a** displayed a remarkable efficacy in killing a broad range of tumor cell models including solid tumors (prostate, bladder, bone, lung, breast, liver) and hematological tumors (CML, AML). The average GI_{50} was below 100 nM (17 to 175 nM range) for all cancer cell models except for the hepatocarcinoma HepG2 cells (GI_{50} = 2.43 μM), a model notoriously known to be refractory to chemotherapy. It should be indeed pointed out that the multikinase inhibitor sorafenib, the standard of care for hepatocarcinoma, displayed an GI_{50} value > 4.1 μM on the HepG2 cell line. Importantly, for all tested cancer cell models, complex **2a** outperformed the drugs of reference used in this study, namely auranofin and DHA, both of which have been proposed for drug repurposing in cancer and are currently used in several phase I/II and phase II/III clinical trials (source: National Cancer Institute). Of note, complex **2a** also presented a better specificity than auranofin and DHA for cancer cells vis-à-vis non cancer models (epithelial cells, osteoblasts and fibroblasts).

Interestingly, complex **2a** could overcome the multidrug resistance phenotype observed in malignant AML HL-60 cells exposed to anthracyclines (doxorubicin) or plant-based alkaloids (etoposide), which remains a major obstacle to successful chemotherapy. The development of refractory disease in AML is frequently correlated with the expression of one or several multidrug resistance (MDR) genes, such as MDR1 or MRP1 [54], which are notably target genes of the transcription factor NRF2 [28] studied in this work.

Although complex **2a** share some common features with auranofin or DHA regarding its impact on TrxR inhibition or ROS production, its mechanism of action appears quite distinctive. Similarly to auranofin or DHA, complex **2a** could inhibit NF-κB and HIF (Hypoxia Inducible Factor) activities, yet in a steadily efficacy. With regard to NF-κB signaling, complex **2a** surpassed the well-established effect of auranofin, which has been originally described as an anti-inflammatory drug (IC_{50} of 627 nM versus 2.97 μM in our cell model). Interestingly, one can speculate that the effect of complex **2a** is likely related to its NHC scaffold of a bisNHC gold(I) complex, as complex **3** (IC_{50} of 664 nM). The efficacy of complex **2a** could give support for its investigation as a potential drug in inflammation-related pathological conditions. Complex **2a** strongly inhibited the transcriptional activity of HIF (Hypoxia Inducing Factor) with an IC_{50} value close to that of auranofin, suggesting a possible mutual mechanism of action that could be related to Au(I) rather than the NHC scaffold since complex **3** was less active in inhibiting HIF transcriptional activity. The literature about the effect of auranofin on hypoxia is scarce and mostly indirect, and nothing is known about the effect of NHC gold(I) complexes on HIF signaling. Certainly, the data presented in this work demonstrate that the impact of gold(I) related compounds is presumably underestimated in pathologies associated with hypoxia.

While auranofin, DHA or the NHC scaffold of a bisNHC gold(I) stimulated NRF2 activity, complex **2a** remarkably impeded NRF2 activity in two different cellular models (liver and lung), with an inhibitory effect seen at all tested concentrations as low as nM concentrations. The mechanism(s) of action of our complex **2a** towards NRF2 signaling is unknown and will be investigated in details in future studies. If NRF2 is normally beneficial, cancer cells can support their malignant progression through various mechanisms leading

to its constitutive activation. These mechanisms leading to NRF2 activation include somatic mutations of *KEAP1* and *NRF2* genes, aberrant activation of the p62/SQSTM1, epigenetic silencing of the *KEAP1* and *CUL3* genes and oncogene-mediated transcriptional upregulation of the *NRF2* gene [22, 55]. Overall, cancer cells expressing high levels of NRF2 can undergo metabolic reprogramming [56] that drives aggressiveness and resistance to anticancer therapies, with tumors more difficult to manage clinically [22, 55].

The elevated activity of NRF2 in cancer cells has been shown to decreased the sensitivity to ionizing radiations and common chemotherapies. In this regard, hepatocarcinoma is an ideal example as KEAP1/NRF2 has been shown to be one of the most frequently mutated pathways in this tumor location [57]. Our data reveal that complex **2a** dramatically sensitizes to sorafenib in the HepG2 liver cells, where aberrant NRF2 activity is further amplified by sorafenib. There was a stunning synergy of effect when complex **2a** was combined to sorafenib, certainly indicating that inhibition of NRF2 activity by complex **2a** counteracts this mechanism of resistance hereby sensitizing hepatocarcinoma cells to sorafenib. Our data potentially sheds light on complex **2a** as a potential sorafenib sensitizing agent to allow more effective therapeutic regimens designed for hepatocarcinoma patients. The inhibition of NRF2 signaling is therefore highly desirable in cancer to improve the efficacy of the treatments. Brusatol, a component of the *Brucea javanica* plant, has been identified as a potential inhibitor of NRF2 by enhancing its ubiquitination, and enhancing efficacy of chemotherapy in lung cancer models [58]. However, brusatol is not specific to NRF2 and is more a global protein synthesis inhibitor [59]. The search for inhibitors of a transcription factor such as NRF2 remains a major challenge in pharmacology as transcription factors are typically considered "undruggable" [60].

The mechanism(s) by which complex **2a** inhibits three majors NF-κB, HIF and NRF2 transcriptional activities involved in cancer progression and resistance warrants further investigation. A better appreciation of its mechanism(s) of action, notably its unique effect towards NRF2, is needed before we can fully determine its therapeutic value in preclinical models.

Methods

All experimental methods used for the herein described studies are available as Supporting Information.

Acknowledgements

This work was supported by the Centre National de la Recherche Scientifique (CNRS) and CZ thanks the Chinese Scholarship Council (CSC) for PhD fellowship.

References

1. WHO. World malaria report 2019. Geneva: World Health Organization; 2019 4 december 2019.

2. Krishna S, Bustamante L, Haynes RK, Staines HM. Artemisinins: their growing importance in medicine. *Trends Pharmacol Sci* 2008, **29**(10)**:** 520-527.

3. Efferth T. From ancient herb to modern drug: Artemisia annua and artemisinin for cancer therapy. *Semin Cancer Biol* 2017, **46:** 65-83.

4. Efferth T. Beyond malaria: The inhibition of viruses by artemisinin-type compounds. *Biotechnol Adv* 2018, **36**(6)**:** 1730-1737.

5. Wong YK, Xu C, Kalesh KA, He Y, Lin Q, Wong WSF*, et al.* Artemisinin as an anticancer drug: Recent advances in target profiling and mechanisms of action. *Med Res Rev* 2017, **37**(6)**:** 1492-1517.

6. Zhang CJ, Wang J, Zhang J, Lee YM, Feng G, Lim TK*, et al.* Mechanism-Guided Design and Synthesis of a Mitochondria-Targeting Artemisinin Analogue with Enhanced Anticancer Activity. *Angew Chem Int Ed Engl* 2016, **55**(44)**:** 13770-13774.

7. Eling N, Reuter L, Hazin J, Hamacher-Brady A, Brady NR. Identification of artesunate as a specific activator of ferroptosis in pancreatic cancer cells. *Oncoscience* 2015, **2**(5)**:** 517-532.

8. Ooko E, Saeed ME, Kadioglu O, Sarvi S, Colak M, Elmasaoudi K*, et al.* Artemisinin derivatives induce iron-dependent cell death (ferroptosis) in tumor cells. *Phytomedicine* 2015, **22**(11)**:** 1045-1054.

9. Zou T, Lok CN, Wan PK, Zhang ZF, Fung SK, Che CM. Anticancer metal-N-heterocyclic carbene complexes of gold, platinum and palladium. *Curr Opin Chem Biol* 2018, **43:** 30-36.

10. Jurgens S, Casini A. Mechanistic Insights into Gold Organometallic Compounds and their Biomedical Applications. *Chimia (Aarau)* 2017, **71**(3)**:** 92-101.

11. Porchia M, Pellei M, Marinelli M, Tisato F, Del Bello F, Santini C. New insights in Au-NHCs complexes as anticancer agents. *Eur J Med Chem* 2018, **146:** 709-746.

12. Liu W, Gust R. Update on metal N-heterocyclic carbene complexes as potential anti-tumor metallodrugs. *Coord Chem Rev* 2016, **329:** 191-213.

13. Boselli L, Ader I, Carraz M, Hemmert C, Cuvillier O, Gornitzka H. Synthesis, structures, and selective toxicity to cancer cells of gold(I) complexes involving N-heterocyclic carbene ligands. *Eur J Med Chem* 2014, **85:** 87-94.

14. Zhang C, Hemmert C, Gornitzka H, Cuvillier O, Zhang M, Sun RW. Cationic and Neutral N-Heterocyclic Carbene Gold(I) Complexes: Cytotoxicity, NCI-60 Screening, Cellular Uptake, Inhibition of Mammalian Thioredoxin Reductase, and Reactive Oxygen Species Formation. *ChemMedChem* 2018, **13**(12)**:** 1218-1229.

15. Zhang C, Maddelein ML, Wai-Yin Sun R, Gornitzka H, Cuvillier O, Hemmert C. Pharmacomodulation on Gold-NHC complexes for anticancer applications - is lipophilicity the key point? *Eur J Med Chem* 2018, **157:** 320-332.

16. Haynes RK, Chan HW, Cheung MK, Lam WL, Soo MK, Tsang HW*, et al.* C-10 Ester and Ether Derivatives of Dihydroartemisinin−10-α Artesunate, Preparation of Authentic 10-β Artesunate, and of Other Ester and Ether Derivatives Bearing Potential Aromatic Intercalating Groups at C-10. *Eur J Org Chem* 2002(1)**:** 113-132.

17. Roder C, Thomson MJ. Auranofin: repurposing an old drug for a golden new age. *Drugs R D* 2015, **15**(1)**:** 13-20.

18. Paloque L, Hemmert C, Valentin A, Gornitzka H. Synthesis, characterization, and antileishmanial activities of gold(I) complexes involving quinoline functionalized N-heterocyclic carbenes. *Eur J Med Chem* 2015, **94:** 22-29.

19. Franken NA, Rodermond HM, Stap J, Haveman J, van Bree C. Clonogenic assay of cells in vitro. *Nat Protoc* 2006, **1**(5)**:** 2315-2319.

20. Ikeda M, Morizane C, Ueno M, Okusaka T, Ishii H, Furuse J. Chemotherapy for hepatocellular carcinoma: current status and future perspectives. *Jpn J Clin Oncol* 2018, **48**(2)**:** 103-114.

21. Gorrini C, Harris IS, Mak TW. Modulation of oxidative stress as an anticancer strategy. *Nat Rev Drug Discov* 2013, **12**(12)**:** 931-947.

22. Yamamoto M, Kensler TW, Motohashi H. The KEAP1-NRF2 System: a Thiol-Based Sensor-Effector Apparatus for Maintaining Redox Homeostasis. *Physiol Rev* 2018, **98**(3)**:** 1169-1203.

23. Tanaka G, Inoue K, Shimizu T, Akimoto K, Kubota K. Dual pharmacological inhibition of glutathione and thioredoxin systems synergizes to kill colorectal carcinoma stem cells. *Cancer Med* 2016, **5**(9)**:** 2544-2557.

24. Raninga PV, Di Trapani G, Vuckovic S, Tonissen KF. Cross-talk between two antioxidants, thioredoxin reductase and heme oxygenase-1, and therapeutic implications for multiple myeloma. *Redox Biol* 2016, **8:** 175-185.

25. Chen W, Li S, Li J, Zhou W, Wu S, Xu S*, et al.* Artemisitene activates the Nrf2-dependent antioxidant response and protects against bleomycin-induced lung injury. *FASEB J* 2016, **30**(7)**:** 2500-2510.

26. Roh JL, Kim EH, Jang H, Shin D. Nrf2 inhibition reverses the resistance of cisplatin-resistant head and neck cancer cells to artesunate-induced ferroptosis. *Redox Biol* 2017, **11:** 254-262.

27. Oommen D, Yiannakis D, Jha AN. BRCA1 deficiency increases the sensitivity of ovarian cancer cells to auranofin. *Mutat Res* 2016, **784-785:** 8-15.

28. Bai X, Chen Y, Hou X, Huang M, Jin J. Emerging role of NRF2 in chemoresistance by regulating drug-metabolizing enzymes and efflux transporters. *Drug Metab Rev* 2016, **48**(4)**:** 541-567.

29. Szakacs G, Paterson JK, Ludwig JA, Booth-Genthe C, Gottesman MM. Targeting multidrug resistance in cancer. *Nat Rev Drug Discov* 2006, **5**(3)**:** 219-234.

30. Bonhoure E, Pchejetski D, Aouali N, Morjani H, Levade T, Kohama T*, et al.* Overcoming MDR-associated chemoresistance in HL-60 acute myeloid leukemia cells by targeting sphingosine kinase-1. *Leukemia* 2006, **20**(1)**:** 95-102.

31. Wu CH, Rastegar M, Gordon J, Safa AR. beta(2)-microglobulin induces apoptosis in HL-60 human leukemia cell line and its multidrug resistant variants overexpressing MRP1 but lacking Bax or overexpressing P-glycoprotein. *Oncogene* 2001, **20**(48)**:** 7006-7020.

32. Totoki Y, Tatsuno K, Covington KR, Ueda H, Creighton CJ, Kato M*, et al.* Trans-ancestry mutational landscape of hepatocellular carcinoma genomes. *Nat Genet* 2014, **46**(12)**:** 1267-1273.

33. Schulze K, Imbeaud S, Letouze E, Alexandrov LB, Calderaro J, Rebouissou S*, et al.* Exome sequencing of hepatocellular carcinomas identifies new mutational signatures and potential therapeutic targets. *Nat Genet* 2015, **47**(5)**:** 505-511.

34. Sun X, Ou Z, Chen R, Niu X, Chen D, Kang R*, et al.* Activation of the p62-Keap1-NRF2 pathway protects against ferroptosis in hepatocellular carcinoma cells. *Hepatology* 2016, **63**(1)**:** 173-184.

35. Bai T, Lei P, Zhou H, Liang R, Zhu R, Wang W*, et al.* Sigma-1 receptor protects against ferroptosis in hepatocellular carcinoma cells. *J Cell Mol Med* 2019, **23**(11)**:** 7349-7359.

36. Zhao L, Au JL, Wientjes MG. Comparison of methods for evaluating drug-drug interaction. *Front Biosci (Elite Ed)* 2010, **2:** 241-249.

37. Xia Y, Shen S, Verma IM. NF-kappaB, an active player in human cancers. *Cancer Immunol Res* 2014, **2**(9)**:** 823-830.

38. Ben-Neriah Y, Karin M. Inflammation meets cancer, with NF-kappaB as the matchmaker. *Nat Immunol* 2011, **12**(8)**:** 715-723.

39. Wang CY, Cusack JC, Jr., Liu R, Baldwin AS, Jr. Control of inducible chemoresistance: enhanced anti-tumor therapy through increased apoptosis by inhibition of NF-kappaB. *Nat Med* 1999, **5**(4)**:** 412-417.

40. Nakaya A, Sagawa M, Muto A, Uchida H, Ikeda Y, Kizaki M. The gold compound auranofin induces apoptosis of human multiple myeloma cells through both down-regulation of STAT3 and inhibition of NF-kB activity. *Leuk Res* 2011, **35**(2)**:** 243-249.

41. Kiebala M, Skalska J, Casulo C, Brookes PS, Peterson DR, Hilchey SP*, et al.* Dual targeting of the thioredoxin and glutathione antioxidant systems in malignant B cells: a novel synergistic therapeutic approach. *Exp Hematol* 2015, **43**(2)**:** 89-99.

42. Raninga PV, Di Trapani G, Vuckovic S, Tonissen KF. TrxR1 inhibition overcomes both hypoxia-induced and acquired bortezomib resistance in multiple myeloma through NF-kB inhibition. *Cell Cycle* 2016, **15**(4)**:** 559-572.

43. Thanaketpaisarn O, Waiwut P, Sakurai H, Saiki I. Artesunate enhances TRAIL-induced apoptosis in human cervical carcinoma cells through inhibition of the NF-kappaB and PI3K/Akt signaling pathways. *Int J Oncol* 2011, **39**(1)**:** 279-285.

44. Wang SJ, Gao Y, Chen H, Kong R, Jiang HC, Pan SH*, et al.* Dihydroartemisinin inactivates NF-kappaB and potentiates the anti-tumor effect of gemcitabine on pancreatic cancer both in vitro and in vivo. *Cancer Lett* 2010, **293**(1)**:** 99-108.

45. Jiang J, Geng G, Yu X, Liu H, Gao J, An H*, et al.* Repurposing the anti-malarial drug dihydroartemisinin suppresses metastasis of non-small-cell lung cancer via inhibiting NF-kappaB/GLUT1 axis. *Oncotarget* 2016, **7**(52)**:** 87271-87283.

46. Nunes JJ, Pandey SK, Yadav A, Goel S, Ateeq B. Targeting NF-kappa B Signaling by Artesunate Restores Sensitivity of Castrate-Resistant Prostate Cancer Cells to Antiandrogens. *Neoplasia* 2017, **19**(4)**:** 333-345.

47. Semenza GL. Hypoxia-inducible factors in physiology and medicine. *Cell* 2012, **148**(3)**:** 399-408.

48. Vaupel P, Mayer A. Hypoxia in cancer: significance and impact on clinical outcome. *Cancer Metastasis Rev* 2007, **26**(2)**:** 225-239.

49. Wang H, Bouzakoura S, de Mey S, Jiang H, Law K, Dufait I*, et al.* Auranofin radiosensitizes tumor cells through targeting thioredoxin reductase and resulting overproduction of reactive oxygen species. *Oncotarget* 2017, **8**(22)**:** 35728-35742.

50. Rios Perez MV, Roife D, Dai B, Pratt M, Dobrowolski R, Kang Y*, et al.* Antineoplastic effects of auranofin in human pancreatic adenocarcinoma preclinical models. *Surgery Open Science* 2019, **1**(2)**:** 56-63.

51. Vandewynckel YP, Laukens D, Geerts A, Vanhove C, Descamps B, Colle I*, et al.* Therapeutic effects of artesunate in hepatocellular carcinoma: repurposing an ancient antimalarial agent. *Eur J Gastroenterol Hepatol* 2014, **26**(8)**:** 861-870.

52. Huang XJ, Ma ZQ, Zhang WP, Lu YB, Wei EQ. Dihydroartemisinin exerts cytotoxic effects and inhibits hypoxia inducible factor-1alpha activation in C6 glioma cells. *J Pharm Pharmacol* 2007, **59**(6)**:** 849-856.

53. Wu XH, Zhou HJ, Lee J. Dihydroartemisinin inhibits angiogenesis induced by multiple myeloma RPMI8226 cells under hypoxic conditions via downregulation of vascular endothelial growth factor expression and suppression of vascular endothelial growth factor secretion. *Anticancer Drugs* 2006, **17**(7)**:** 839-848.

54. Sonneveld P. Multidrug resistance in haematological malignancies. *J Intern Med* 2000, **247**(5)**:** 521-534.

55. Suzuki T, Motohashi H, Yamamoto M. Toward clinical application of the Keap1-Nrf2 pathway. *Trends Pharmacol Sci* 2013, **34**(6)**:** 340-346.

56. Mitsuishi Y, Taguchi K, Kawatani Y, Shibata T, Nukiwa T, Aburatani H*, et al.* Nrf2 redirects glucose and glutamine into anabolic pathways in metabolic reprogramming. *Cancer Cell* 2012, **22**(1)**:** 66-79.

57. Nault JC, Rebouissou S, Zucman Rossi J. NRF2/KEAP1 and Wnt/beta-catenin in the multistep process of liver carcinogenesis in humans and rats. *Hepatology* 2015, **62**(3)**:** 677-679.

58. Ren D, Villeneuve NF, Jiang T, Wu T, Lau A, Toppin HA*, et al.* Brusatol enhances the efficacy of chemotherapy by inhibiting the Nrf2-mediated defense mechanism. *Proc Natl Acad Sci U S A* 2011, **108**(4)**:** 1433-1438.

59. Harder B, Tian W, La Clair JJ, Tan AC, Ooi A, Chapman E*, et al.* Brusatol overcomes chemoresistance through inhibition of protein translation. *Mol Carcinog* 2017, **56**(5)**:** 1493-1500.

60. Bushweller JH. Targeting transcription factors in cancer - from undruggable to reality. *Nat Rev Cancer* 2019, **19**(11)**:** 611-624.

Artemisinin-Derivative-NHC-gold(I)-Hybrid with enhanced cytotoxic activity through inhibiting NRF2 transcriptional activity

Chen Zhang[1,2,$], Pierre-Yves Fortin[2,$], Guillaume Barnoin[1,$], Xue Qin[1], Xing Wang[1], Alvaro Fernandez Alvarez[1], Christian Bijani[1], Marie-Lise Maddelein[2], Catherine Hemmert[1,*], Olivier Cuvillier[2,*], Heinz Gornitzka[1,*]

[1] LCC-CNRS, Université de Toulouse, CNRS, UPS, Toulouse, France

E-mail: hemmert@lcc-toulouse.fr and gornitzka@lcc-toulouse.fr

[2] Institut de Pharmacologie et de Biologie Structurale, Université de Toulouse, CNRS, UPS, Toulouse, France

E-mail: olivier.cuvillier@inserm.fr

[$] These authors contributed equally to this work.

Experimental section

Chemistry

1. General information……...…….……...S3

2. Synthesis of proligands **1a-c** and complexes **2a-c**…….……S3

2.1. Synthesis of proligands **1a-c**…….……..S3

2.2. Synthesis of complexes **2a-c**..……S8

3. Crystallographic data for **2a**……..……..S10

Biology

1. Cell culture…….…….S10

2. Cell viability assay (MTT assay)…….S11

3. Clonogenic assay …….…….....S12

4. Measurement of intracellular reactive oxygen species (ROS)…….S12

5. NRF2 transcriptional activity in MCF-7 and HepG2 cells……..……S12

6. NF-κB transcriptional activity……..…S13

7. HIF transcriptional activity……..S14

8. Isobologram construction S14

9. Inhibition of mammalian TrxR……. ……S15
References…….S15
^{1}H and ^{13}C NMR spectra of compounds **DHA-C3-C5**, **1a-c** and **2a-c**; ^{1}H-^{1}H COSY, ^{1}H-^{13}C HSQC/HMBC and ^{1}H-^{13}C HMBC spectra of **2a-c**…….S17
Supplementary Figure 1. Colony formation in bladder cancer T24 (top) and prostate cancer PC-3 (bottom) cells treated with increasing concentrations of complex **2a** for 24 h and stained with crystal violet after 1 week of cultivation…….....S31
Supplementary Figure 2. ROS generation of DHA, Auranofin and **2a** on a representative panel of cancer cell lineages (DCFH-DA assay)…….….S32
Supplementary Figure 3. Inhibitory effects of Auranofin, DHA, 3 and **2a** compounds on NF-κB and HIF transcriptional activities in A549 and HeLa cancer cell models, respectively.
a, kinetic of NF-κB activation by TNFα in A549 lung cancer cell model in which NF-κB luciferase reporter construct is stably integrated; b, the NF-κB inhibitory effect of the described compounds was evaluated in NF-κB /A549 reporter activity in response to 7h of treatment with TNFα; c, the HIF inhibitory effect of the described compounds was evaluated in HIF Luciferase Reporter Hela in response to hypoxia (0.1% O_2)…….……...S33
Supplementary Figure 4: IC_{50} values of complex **2a** towards isolated mammalian TrxR….S34

Experimental section

Chemistry

1. General information

All complexation reactions were performed under an inert atmosphere of dry nitrogen by using standard vacuum line and Schlenk tube techniques. Reactions involving silver compounds were performed with the exclusion of light. CH_3CN was dried over CaH_2 and subsequently distilled. 10β-(20-Bromopropoxy)dihydroartemisinin (**DHA-C3**) was synthetized according a modified literature procedure [1]. All other reagents were used as received from commercial suppliers. ^1H (300 or 400 MHz) and ^{13}C NMR spectra (75 or 101 MHz) and 2D experiments were recorded at 298 K on Bruker AV300, Bruker AV400 or Bruker Avance 500 spectrometers in $CDCl_3$ as solvent. All chemical shifts for ^1H and ^{13}C are relative to TMS using ^1H (residual) or ^{13}C chemical shifts of the solvent as a secondary standard. All the ^1H and ^{13}C signals were assigned based on chemical shifts, spin-spin coupling constants, splitting patterns and signal intensities, and by using ^1H-^1H COSY45, ^1H-^{13}C HMBC and ^1H-^{13}C HSQC/HMQC, experiments for complexes **2a-2c**. Gradient-enhanced ^1H COSY45 was realised included 2 scans for per increment. ^1H-^{13}C correlation spectra using a gradient-enhanced HSQC/HMQC sequence (delay was optimised for $^1J_{CH}$ of 145 Hz) was obtained with 2 scans per increment. Gradient-enhanced HMBC experiment was performed allowing 62.5 ms for long-range coupling evolution (8 scans were accumulated). Typically, 1024 t2 data points were collected for 256 t1 increments. High Resolution Mass Spectrometry (HRMS) analysis were performed with a Xévo G2 QTOF Waters spectrometer using electrospray ionization (ESI) by the "Service de Spectrométrie de Masse de Chimie UPS-CNRS (Toulouse)". Elemental analyses were carried out by the “Service de Microanalyse du Laboratoire de Chimie de Coordination (Toulouse)”. The absorbance for MTT assay was measured using a Promega E7031 microplate reader.

2. Synthesis of proligands 1a-c and complexes 2a-c

2.1. Synthesis of proligands 1a-c

The following picture describes the numbering of H (^1H NMR) and C (^{13}C NMR). These notations are used in the following experimental section.

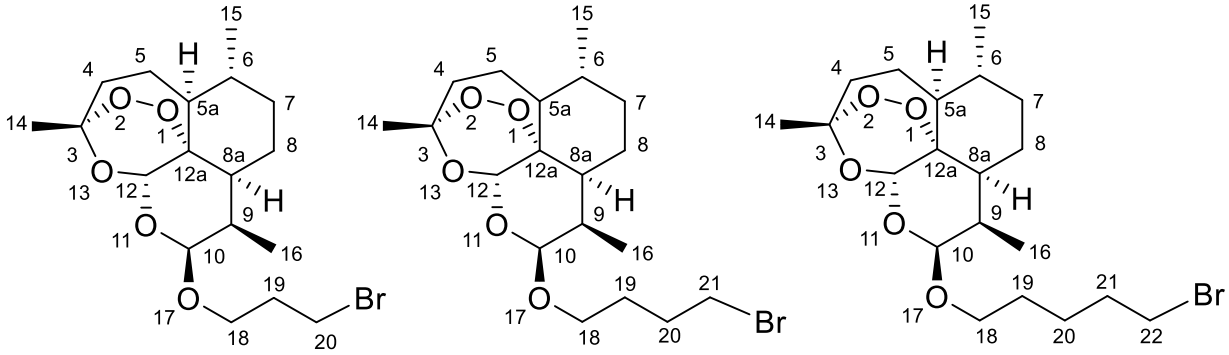

DHA-C3 **DHA-C4** **DHA-C5**

10β-(20-Bromopropoxy)dihydroartemisinin **(DHA-C3)**[1]

Under a nitrogen atmosphere, dihydroartemisinin (DHA) (2 g, 7.0 mmol) was dissolved in 200 mL Et_2O. 3-Bromopropan-1-ol (0.76 mL, 8.4 mmol, 1.2 eq.) and $BF_3{\cdot}Et_2O$ (6 drops) were added and the reaction mixture was stirred for 4 h at room temperature. Then the solution was treated with a saturated solution of $NaHCO_3$ and the product was extracted with Et_2O (3 x 20 mL). The combined organic phases were dried over Na_2CO_3, filtered and the solvent was evaporated to dryness. The crude product was purified by column chromatography on silica using hexane-ethyl acetate as eluent (100/0 to 100/20) to give a white solid (1.277 g, 45 % yield). ^{1}H NMR (400 MHz, $CDCl_3$): δ = 5.44 (s, 1H, H12), 4.82 (d, J = 3.4 Hz, 1H, H10), 4.04-3.97 (m, 1H, H18), 3.54-3.47 (m, 3H, H18, H20), 2.70-2.60 (m, 1H, H9), 2.43-2.33 (m, 1H, H4), 2.15-2.06 (m, 2H, H19), 2.03-2.01 (m, 1H, H4), 1.94-1.85 (m, 1H, H5), 1.80-1.72 (m, 2H, H8), 1.68-1.62 (m, 1H, H7), 1.54-1.50 (m, 1H, H8a), 1.49-1.47 (m, 1H, H5), 1.46 (s, 3H, H14), 1.37-1.30 (m, 1H, H6), 1.29-1.23 (m, 1H, H5a), 0.97 (d, J = 6.3 Hz, 3H, H15), 0.94-0.89 (m, 1H, H7), 0.92 (d, J = 7.4 Hz, 3H, H16). ^{13}C NMR (75 MHz, $CDCl_3$): δ = 104.05 (1C, C3), 102.07 (1C, C10), 87.89 (1C, C12), 80.99 (1C, C12a), 65.66 (1C, C18), 52.56 (1C, C5a), 44.36 (1C, C8a), 37.42 (1C, C6), 36.40 (1C, C4), 34.62 (1C, C7), 32.52 (1C, C19), 30.86 (1C, C9), 30.57 (1C, C20), 26.16 (1C, C14), 24.65-24.49 (2C, C5, C8), 20.35 (1C, C15), 12.96 (1C, C16).

10β-(21-Bromobutoxy)dihydroartemisinin **(DHA-C4)**

Under a nitrogen atmosphere, dihydroartemisinin (DHA, 500 mg, 1.76 mmol) was dissolved in 200 mL Et_2O. 4-Bromobutan-1-ol (398 mg, 2.6 mmol, 1.48 eq.) and $BF_3{\cdot}Et_2O$ (6 drops) were added and the reaction mixture was stirred for 4 h at room temperature. Then the solution was treated with a saturated solution of $NaHCO_3$ and the product was extracted with Et_2O (3 x 20

mL). The combined organic phases were dried over Na_2CO_3, filtered and the solvent was evaporated to dryness. The crude product was purified by column chromatography on silica using hexane-ethyl acetate as eluent (100/0 to 100/20) to give a white solid (220.3 mg, 29 % yield). Anal. Calcd. for $C_{19}H_{31}BrO_5$: C, 54.42; H, 7.45. Found: C, 54.36; H, 7.38. ^{1}H NMR (400 MHz, $CDCl_3$): δ = 5.40 (s, 1H, H12), 4.80 (d, J = 3.2 Hz, 1H, H10), 3.9-3.88 (m, 1H, H18), 3.50-3.36 (m, 3H, H18, H21), 2.71-2.59 (m, 1H, H9), 2.45-2.32 (m, 1H, H4), 2.08-2.03 (m, 1H, H4), 1.99-1.86 (m, 3H, H19, H5), 1.83-1.74 (m, 4H, H8, H20), 1.70-1.63 (m, 1H, H7), 1.56-1.53 (m, 1H, H8a), 1.51-1.49 (m, 1H, H5), 1.46 (s, 3H, H14), 1.38-1.32 (m, 1H, H6), 1.30-1.26 (m, 1H, H5a), 0.98 (d, J = 6.3 Hz, 3H, H15), 0.97-0.95 (m, 1H, H7), 0.92 (d, J = 7.4 Hz, 3H, H16). ^{13}C NMR (101 MHz, $CDCl_3$): δ = 104.10 (1C, C3), 102.02 (1C, C10), 87.92 (1C, C12), 81.10 (1C, C12a), 67.44 (1C, C18), 52.58 (1C, C5a), 44.42 (1C, C8a), 37.49 (1C, C6), 36.44 (1C, C4), 34.64 (1C, C7), 33.63 (1C, C21), 30.90 (1C, C9), 29.83 (1C, C19), 28.34 (1C, C20), 26.22 (1C, C14), 24.69-24.51 (2C, C5, C8), 20.37 (1C, C15), 13.04 (1C, C16). HRMS (ES^+): calcd. for $C_{19}H_{31}BrNaO_5$ m/z = 441.1253; found 441.1251.

10β-(22-Bromopentoxy)dihydroartemisinin **(DHA-C5)**

Under a nitrogen atmosphere, dihydroartemisinin (DHA, 1 g, 3.5 mmol) was dissolved in 200 mL Et_2O. 5-Bromopentan-1-ol (601 mg, 3.6 mmol, 1.03 eq.) and $BF_3{\cdot}Et_2O$ (6 drops) were added and the reaction mixture was stirred for 4 h at room temperature. Then the solution was treated with a saturated solution of $NaHCO_3$ and the product was extracted with Et_2O (3 x 20 mL). The combined organic phases were dried over Na_2CO_3, filtered and the solvent was evaporated to dryness. The crude product was purified by column chromatography on silica using hexane-ethyl acetate as eluent (100/0 to 100/20) to give a white solid (314.4 mg, 21 % yield). Anal. Calcd. for $C_{20}H_{33}BrO_5$: C, 55.43; H, 7.68. Found: C, 55.49; H, 7.82. ^{1}H NMR (400 MHz, $CDCl_3$): δ = 5.41 (s, 1H, H12), 4.79 (d, J = 3.2 Hz, 1H, H10), 3.87 (dt, J = 9.8, 6.2 Hz, 1H, H18), 3.45-3.37 (m, 3H, H18, H22), 2.66-2.61 (m, 1H, H9), 2.39 (ddd, J = 14.5, 13.4, 3.9 Hz, 1H, H4), 2.08-2.02 (m, 1H, H4), 1.94-1.87 (3H, H5, H21), 1.82-1.77 (m, 1H, H7), 1.67-1.48 (m, 8H, H5, H8, H8a, H19, H20), 1.50 (s, 3H, H14), 1.40-1.32 (m, 1H, H6), 1.29-1.22 (m, 1H, H5a), 0.97 (d, J = 6.3 Hz, 3H, H15), 0.98-0.91 (m, 1H, H7), 0.92 (d, J = 7.4 Hz, 3H, H16). ^{13}C NMR (101 MHz, $CDCl_3$): δ = 104.05 (1C, C3), 101.99 (1C, C10), 87.92 (1C, C12), 81.12 (1C, C12a), 68.01 (1C, C18), 52.58 (1C, C5a), 44.45 (1C, C8a), 37.46 (1C, C6), 36.44 (1C, C4), 34.66 (1C, C7), 33.81 (1C, C22), 32.41 (1C, C21), 30.92 (1C, C9), 28.82 (1C, C19), 26.21

(1C, C14), 24.96 (1C, C20), 24.68-24.48 (2C, C5, C8), 20.36 (1C, C15), 13.04 (1C, C16). HRMS (ES^+): calcd. for $C_{20}H_{33}BrNaO_5$ m/z = 455.1409; found 455.1409.

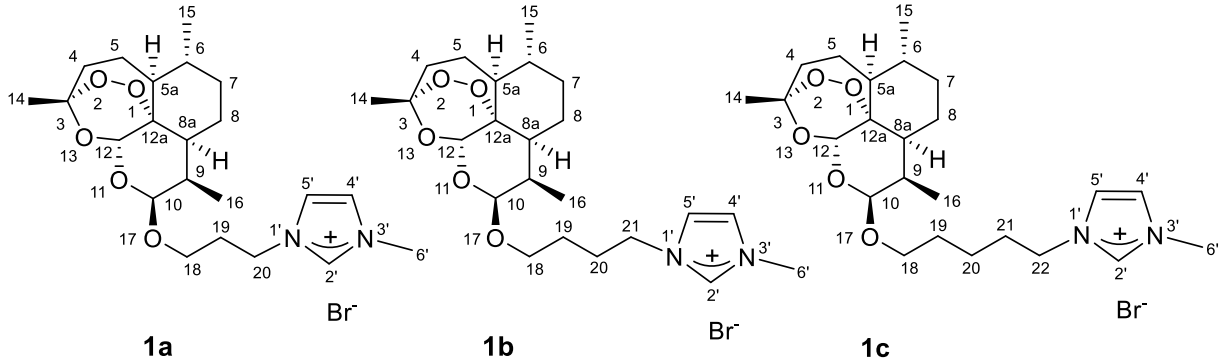

1a **1b** **1c**

3'-methyl-1'-[10β-(20-propoxy)dihydroartemisinin]1H-imidazol-3-ium bromide (**1a**)

To a stirred solution of **DHA-C3** (304 mg, 0.75 mmol) in CH_3CN (6 mL) under reflux, 1-methylimidazole (60 µL, 0.75 mmol) was added and the reaction mixture was stirred 3 days under reflux. The solvent was evaporated under reduced pressure and the viscous residue was purified by chromatography on silica with CH_2Cl_2-MeOH as eluent (1/0.1 to 1/0.25) to afford a white solid (238 mg, 65% yield). Anal. Calcd. for $C_{22}H_{35}BrN_2O_5$: C, 54.21; H, 7.24; N, 5.75. Found C, 54.12; H, 7.26; N, 5.68. ^{1}H NMR (400 MHz, $CDCl_3$): δ = 10.44 (s, 1H, H2'), 7.48 (s, 1H, H4'), 7.38 (s, 1H, H5'), 5.38 (s, 1H, H12), 4.79 (d, J = 3.6 Hz, 1H, H10), 4.44 (t, J = 7.2 Hz, 2H, H20), 4.14 (s, 3H, H6'), 3.92-3.86 (m, 1H, H18), 3.53-3.47 (m, 1H, H18), 2.68-2.61 (m, 1H, H9), 2.37 (ddd, J = 14.6, 13.4, 4.0 Hz, 1H, H4), 2.29-2.22 (m, 2H, H19), 2.04 (ddd, J = 14.6, 4.9, 2.9 Hz, 1H, H4), 1.93-1.86 (m, 1H, H5), 1.81-175 (m, 1H, H7), 1.72-1.61 (m, 2H, H8), 1.51-1.44 (m, 2H, H5, H8a), 1.42 (s, 3H, H14), 1.38-1.31 (m, 1H, H6), 1.29-1.23 (m, 1H, H5a), 0.97 (d, J = 6.3 Hz, 3H, H15), 0.95-0.89 (m, 1H, H7), 0.92 (d, J = 7.4 Hz, 3H, H16). ^{13}C NMR (101 MHz, $CDCl_3$): δ = 137.90 (1C, C2'), 123.37 (1C, C4'), 122.15 (1C, C5'),104.23 (1C, C3), 102.20 (1C, C10), 87.96 (1C, C12), 80.92 (1C, C12a), 64.60 (1C, C18), 52.42 (1C, C5a), 47.48 (1C, C20), 44.16 (1C, C8a), 37.45 (1C, C6'), 36.90 (1C, C6), 36.33 (1C, C4), 34.45 (1C, C7), 30.77 (1C, C9), 30.60 (1C, C19), 26.10 (1C, C14), 24.63-24.57 (2C, C5, C8), 20.29 (1C, C15), 13.13 (1C, C16). HRMS (ES^+): calcd. for $C_{22}H_{35}N_2O_5$ m/z = 407.2545; found 407.2546.

3'-methyl-1'-[10β-(21-butoxy)dihydroartemisinin]1H-imidazol-3-ium bromide (**1b**)

To a stirred solution of **DHA-C4** (75 mg, 0.18 mmol) in CH_3CN (3 mL) under reflux, 1-methylimidazole (57 μL, 0.72 mmol, 4 eq.) was added and the reaction mixture was stirred 5 days under reflux. The solvent was evaporated under reduced pressure and the viscous residue was purified by chromatography on silica with CH_2Cl_2-MeOH as eluent (1/0.1 to 1/0.25) to afford a white solid (83 mg, 92% yield). Anal. Calcd. for $C_{23}H_{37}BrN_2O_5$: C, 55.09; H, 7.44; N, 5.59. Found C, 55.12; H, 7.56; N, 5.58. ^{1}H NMR (400 MHz, $CDCl_3$): δ = 10.38 (s, 1H, H2'), 7.55 (t, 1H, *J* = 1.8 Hz, H4'), 7.42 (t, 1H, *J* = 1.8 Hz, H5'), 5.34 (s, 1H, H12), 4.75 (d, *J* = 3.4 Hz, 1H, H10), 4.37 (t, *J* = 7.4 Hz, 2H, H21), 4.10 (s, 3H, H6'), 3.83 (dt, 1H, *J* = 9.9, 6.0 Hz, H18), 3.40 (dt, 1H, *J* = 9.9, 6.4 Hz, H18), 2.62-2.52 (m, 1H, H9), 2.37-2.29 (m, 1H, H4), 2.04-1.83 (m, 3H, H4, H20), 1.90-1.83 (m, 1H, H5), 1.73-1.59 (m, 5H, H7, H8, H19), 1.51-1.41 (m, 2H, H8a, H5), 1.39 (s, 3H, H14), 1.35-1.27 (m, 1H, H6), 1.25-1.17 (m, 1H, H5a), 0.94 (d, *J* = 6.3 Hz, 3H, H15), 0.91-0.83 (m, 1H, H7), 0.87 (d, *J* = 7.3 Hz, 3H, H16). ^{13}C NMR (101 MHz, $CDCl_3$): δ = 137.95 (1C, C2'), 123.41 (1C, C4'), 121.59 (1C, C5'),104.13 (1C, C3), 102.12 (1C, C10), 87.91 (1C, C12), 81.03 (1C, C12a), 67.43 (1C, C18), 52.49 (1C, C5a), 49.88 (1C, C21), 44.29 (1C, C8a), 37.43 (1C, C6'), 36.82 (1C, C6), 36.38 (1C, C4), 34.51 (1C, C7), 30.84 (1C, C9), 27.28-26.44 (2C, C19, C20), 26.17(1C, C14), 24.65-24.52 (2C, C5, C8), 20.32 (1C, C15), 13.09 (1C, C16). HRMS (ES^+): calcd. for $C_{23}H_{37}N_2O_5$ m/z = 421.2702; found 421.2704.

3'-methyl-1'-[10β-(22-pentoxy)dihydroartemisinin]1H-imidazol-3-ium bromide (**1c**)

To a stirred solution of **DHA-C5** (189 mg, 0.45 mmol) in CH_3CN (6 mL) under reflux, 1-methylimidazole (143 μL, 0.43 mmol, 4 eq.) was added and the reaction mixture was stirred 3 days under reflux. The solvent was evaporated under reduced pressure and the viscous residue was purified by chromatography on silica with CH_2Cl_2-MeOH as eluent (1/0.1 to 1/0.25) to afford a white solid (91 mg, 39% yield). Anal. Calcd. for $C_{24}H_{39}BrN_2O_5$: C, 55.92; H, 7.63; N, 5.43. Found C, 55.86; H, 7.56; N, 5.38. ^{1}H NMR (400 MHz, $CDCl_3$): δ = 10.40 (s, 1H, H2'), 7.54 (t, 1H, *J* = 1.8 Hz, H4'), 7.43 (t, 1H, *J* = 1.8 Hz, H5'), 5.34 (s, 1H, H12), 4.73 (d, *J* = 3.6 Hz, 1H, H10), 4.33 (t, *J* = 7.5 Hz, 2H, H22), 4.12 (s, 3H, H6'), 3.79 (dt, 1H, *J* = 9.8, 6.3 Hz, H18), 3.45 (dt, 1H, *J* = 9.8, 6.5 Hz, H18), 2.62-2.54 (m, 1H, H9), 2.38-2.30 (m, 1H, H4), 2.04-1.92 (m, 3H, H4, H21), 1.89-1.83 (m, 1H, H5), 1.74-1.58 (m, 5H, H7, H8, H19), 1.53-1.37 (m, 4H, H5, H8a, H20), 1.40 (s, 3H, H14), 1.35-1.29 (m, 1H, H6), 1.27-1.18 (m, 1H, H5a), 0.94 (d, *J* = 6.3 Hz, 3H, H15), 0.90-0.83 (m, 1H, H7), 0.86 (d, *J* = 7.3 Hz, 3H, H16). ^{13}C NMR (101 MHz, $CDCl_3$): δ = 137.60 (1C, C2'), 123.51 (1C, C4'), 121.89 (1C, C5'),104.07 (1C, C3),

101.99 (1C, C10), 87.88 (1C, C12), 81.09 (1C, C12a), 67.86 (1C, C18), 52.52 (1C, C5a), 50.00 (1C, C22), 44.37 (1C, C8a), 37.44 (1C, C6'), 36.77 (1C, C6), 36.40 (1C, C4), 34.56 (1C, C7), 30.88 (1C, C9), 30.06-29.01 (2C, C19, C21), 26.19 (1C, C14), 24.66-24.48 (2C, C5, C8), 23.00 (1C, C20), 20.35 (1C, C15), 13.05 (1C, C16). HRMS (ES^+): calcd. for $C_{24}H_{39}N_2O_5$ m/z = 435.2859; found 435.2861.

2.2. Synthesis of complexes 2a-c

Complex **2a**

In a schlenk tube, **1a** (102 mg, 0.21 mmol) and Ag_2O (25 mg, 0.11 mmol) were dissolved in CH_3CN (3 mL) under a nitrogen atmosphere and protection of the light and stirred overnight at room temperature. A solution of $AgNO_3$ (19 mg, 0.11 mmol) in 2 mL of CH_3CN was added and the mixture was stirred for 2 h. Finally, $Au(SMe_2)Cl$ (32 mg, 0.11 mmol) was added and after stirring for 1 h at room temperature, the solution was filtered through a pad of celite and the solvent removed under reduced pressure to afford a white solid (95 mg, 84% yield). Crystals suitable for X-ray diffraction analysis were obtained by slow diffusion of Et_2O in a CH_3CN solution of this complex. Anal. Calcd. For $C_{44}H_{68}AuN_5O_{13}$: C, 49.30; H, 6.39; N, 6.53. Found C, 49.32; H, 6.45; N, 5.49. ^1H NMR (400 MHz, $CDCl_3$): δ 7.26 (d, J = 1.8 Hz, 1H, H4'), 7.16 (d, J = 1.9 Hz, 1H, H5'), 5.37 (s, 1H, H12), 4.79 (d, J = 3.5 Hz, 1H, H10), 4.28 (t, J = 7.0 Hz, 2H, H20), 3.95 (s, 3H, H6'), 3.91-3.89 (m, 1H, H18), 3.46-3.43 (m, 1H, H18), 2.64-2.62 (m, 1H, H9), 2.37-2.34 (m, 1H, H4), 2.19-2.16 (m, 2H, H19), 2.04-2.02 (m, 1H, H4), 1.89-1.87 (m, 1H, H5), 1.73-1.71 (m, 2H, H8), 1.61-1.59 (m, 1H, H7), 1.48-1.46 (m, 1H, H8a), 1.46-1.43 (m, 1H, H5), 1.42 (s, 3H, H14), 1.32-1.30 (m, 1H, H6), 1.25-1.20 (m, 1H, H5a), 0.96 (d, J = 6.2 Hz, 3H, H15), 0.95-0.92 (m, 1H, H7), 0.91 (d, J = 7.4 Hz, 3H, H16). ^{13}C NMR (101 MHz, $CDCl_3$): δ 183.71 (1C, C2'), 123.26 (1C, C4'), 121.84 (1C, C5'), 104.19 (1C, C3), 101.98 (1C, C10), 87.93 (1C, C12), 80.89 (1C, C12a), 64.81 (1C, C18), 52.46 (1C, C5a), 48.50 (1C, C20), 44.22 (1C, C8a), 38.21 (1C, C6'), 37.52 (1C, C6), 36.35 (1C, C4), 34.50 (1C, C7), 31.70 (1C, C19), 30.75 (1C, C9), 26.11 (1C, C14), 24.66-24.54 (2C, C5, C8), 20.31 (1C, C15), 13.10 (1C, C16) HRMS (ES^+): calcd. for $C_{44}H_{68}AuN_4O_{10}$ m/z 1009.4601; found 1009.4591.

Complex **2b**

Under a nitrogen atmosphere, potassium carbonate (27.7 mg, 0.20 mmol) was added to a mixture of **1b** (80 mg, 0.16 mmol) and $Au(SMe_2)Cl$ (26.5 mg, 0.09 mmol) in dry CH_3CN (5

mL). The mixture was then heated to 60 °C and stirred for 2 h. After cooling to room temperature, the solution was filtered through a pad of celite and the solvent removed under reduced pressure. The complex was purified by preparative chromatography on silica plate with CH_2Cl_2-MeOH as eluent (100/8) to afford a white solid (68.7 mg, 80% yield). Anal. Calcd. For $C_{46}H_{72}AuClN_4O_{10}$. C, 51.47; H, 6.76; N, 5.22. Found C, 51.39; H, 6.68; N, 5.18. ^{1}H NMR (400 MHz, $CDCl_3$): δ 7.37 (d, J = 1.9 Hz, 1H, H4'), 7.22 (d, J = 1.9 Hz, 1H, H5'), 5.33 (s, 1H, H12), 4.74 (d, J = 3.2 Hz, 1H, H10), 4.25 (t, J = 7.0 Hz, 2H, H21), 3.97 (s, 3H, H6'), 3.86-3.80 (m, 1H, H18), 3.42-3.37 (m, 1H, H18), 2.61-2.57 (m, 1H, H9), 2.38-2.30 (m, 1H, H4), 2.04-1.84 (m, 4 H, H4, H5, H20), 1.76-1.58 (m, 5H, H7, H8, H19), 1.46-1.37 (m, 2H, H5, H8a), 1.40 (s, 3H, H14), 1.30-1.19 (m, 2H, H5a, H6), 0.94 (d, J = 5.9 Hz, 3H, H15), 0.95-0.84 (m, 1H, H7), 0.86 (d, J = 7.3 Hz, 3H, H16). ^{13}C NMR (101 MHz, $CDCl_3$): δ 183.57 (1C, C2'), 123.45 (1C, C4'), 121.53 (1C, C5'), 104.10 (1C, C3), 101.99 (1C, C10), 87.87 (1C, C12), 80.97 (1C, C12a), 67.50 (1C, C18), 52.40 (1C, C5a), 51.04 (1C, C21), 44.27 (1C, C8a), 38.42 (1C, C6'), 37.49 (1C, C6), 36.35 (1C, C4), 34.53 (1C, C7), 30.79 (1C, C9), 28.34 (1C, C20), 26.73, (1C, C19), 26.16 (1C, C14), 24.65-24.48 (2C, C5, C8), 20.35 (1C, C15), 13.08 (1C, C16) HRMS (ES^+): calcd. for $C_{46}H_{72}AuN_4O_{10}$ m/z 1037.4914; found 1037.4929.

Complex **2c**

Under a nitrogen atmosphere, potassium carbonate (38.7 mg, 0.28 mmol) was added to a mixture of **1c** (118.5 mg, 0.23 mmol) and $Au(SMe_2)Cl$ (35.3 mg, 0.12 mmol) in dry CH_3CN (5 mL). The mixture was then heated to 60 °C and stirred for 2 h. After cooling to room temperature, the solution was filtered through a pad of celite and the solvent removed under reduced pressure. The complex was purified by preparative chromatography on silica plate with CH_2Cl_2-MeOH as eluent (100/8) to afford a white solid (39.3 mg, 31% yield). Anal. Calcd. For $C_{48}H_{76}AuClN_4O_{10}$. C, 52.34; H, 6.95; N, 5.09. Found C, 52.39; H, 6.98; N, 5.08. ^{1}H NMR (300 MHz, $CDCl_3$): δ 7.32 (d, J = 1.9 Hz, 1H, H4'), 7.22 (d, J = 1.9 Hz, 1H, H5'), 5.36 (s, 1H, H12), 4.75 (d, J = 3.6 Hz, 1H, H10), 4.25 (t, J = 7.0 Hz, 2H, H22), 3.99 (s, 3H, H6'), 3.88-3.78 (m, 1H, H18), 3.41-3.33 (m, 1H, H18), 2.63-2.58 (m, 1H, H9), 2.43-2.32 (m, 1H, H4), 2.08-1.97 (m, 4H, H4, H5, H21), 1.78-1.59 (m, 5H, H7, H8, H19), 1.53-1.38 (m, 7H, H5, H8a, H20), 1.43 (s, 3H, H14), 1.30-1.24 (m, 2H, H5a, H6), 0.97 (d, J = 6.1 Hz, 3H, H15), 0.97-0.84 (m, 1H, H7), 0.87 (d, J = 7.4 Hz, 3H, H16). ^{13}C NMR (101 MHz, $CDCl_3$): δ 183.59 (1C, C2'), 123.28 (1C, C4'), 121.65 (1C, C5'), 104.08 (1C, C3), 101.91 (1C, C10), 87.86 (1C, C12), 81.01 (1C,

C12a), 67.85 (1C, C18), 52.49 (1C, C5a), 51.22 (1C, C22), 44.32 (1C, C8a), 38.38 (1C, C6'), 37.48 (1C, C6), 36.37 (1C, C4), 34.58 (1C, C7), 31.22 (1C, C21), 30.82 (1C, C9), 29.13 (1C, C19), 26.18 (1C, C14), 24.66-24.46 (2C, C5, C8), 23.23 (1C, C20), 20.37 (1C, C15), 13.02 (1C, C16) HRMS (ES^+): calcd. for $C_{48}H_{76}AuN_4O_{10}$ m/z 1065.5221; found 1065.5226.

3. Crystallographic data for 2a

All data were collected at low temperature using oil-coated shock-cooled crystals on a Bruker-AXS APEX II diffractometer with MoKa radiation (λ = 0.71073 Å). The structure was solved by direct methods [2] and all non hydrogen atoms were refined anisotropically using the least-squares method on F^2 [3]. The absolute structure parameters have been refined using the Flack-method. CCDC-1978195 contain the additional crystallographic data. These data can be obtained free of charge from the Cambridge Crystallographic Data Centre via www.ccdc.cam.ac.uk/data_request/cif.

Complex 2a: $C_{44}H_{68}AuN_5O_{13.12}$, Mr = 1074.0, crystal size = 0.40 x 0.30 x 0.05 mm^3, orthorhombic, space group *I222*, *a* = 10.644(2) Å, *b* = 19.073(3) Å, *c* = 48.320(8) Å, V = 9809(3) $Å^3$, Z = 8, 59886 reflections collected, 6963 unique reflections (R_{int} = 0.1151), R1 = 0.0568, wR2 = 0.1300 [I>2σ(I)], R1 = 0.1309, wR2 = 0.1727 (all data), absolute structure factor x = -0.021(8), residual electron density = 3.308 e $Å^{-3}$.

Biology

1. Cell culture

Cell lines were obtained from DSMZ (Braunschweig, Germany) or ATCC (Molsheim, France). Culture medium and antibiotics were from Lonza (Basel, Switzerland). Serum was from Perbio (Brebières, France).

PC-3 human prostate cancer cells, and LAMA chronic myeloid leukemia were cultured in RPMI 1640 containing 10% fetal bovine serum (FBS) and 1% antibiotics (100 U/mL penicillin and 100 µg/mL streptomycin) at 37 °C in 5% CO_2 humidified incubators. HL-60 acute myeloid leukemia were cultured in RPMI 1640 containing 15% FBS and 1% antibiotics at 37 °C in 5% CO_2 humidified incubators. HL-60/Doxo resistant cells (gift of Dr. JP. Marie, Hôtel Dieu, Paris, France) were grown in the same medium supplemented with 40 nM doxorubicin [4, 5]. The selection of HL-60/VP16 cells was performed by stepwise increasing concentrations of etoposide, and cells were maintained continuously in the presence of 1 µM VP16. HepG2

human liver cancer cells were cultured in EMEM containing 10% FBS, 1% of nonessential amino acids, 1 mM of Na-pyruvate, 1% antibiotics and 600 µg/mL of Geneticin. MCF-7 human breast adenocarcinoma cells were cultured in Advanced MEM containing 10% FBS, 2 mM glutamine, 1% antibiotics and 2µg/mL of puromycin. A549 human lung carcinoma cells, T24 human bladder carcinoma cells, U-2 OS human osteosarcoma and NIH3T3 murine fibroblast cells were cultured in DMEM medium containing 10% FBS and 1% antibiotics at 37 °C in 5% CO_2 humidified incubators. MC3T3 mouse osteoblast cells were cultured in alpha-MEM medium containing 10% FBS and 1% antibiotics at 37 °C in 5% CO_2 humidified incubators. RWPE-1 human prostate normal cells were cultured in K-SFM medium containing 0.05 mg/ml bovine pituitary extract (BPE) and 5 ng/ml epidermal growth factor (EGF) at 37 °C in 5% CO_2 humidified incubators.

All experiments were started with low-passaged cells (<15 times). Hypoxia (0.1% O_2, 5% CO_2, 94.5% N_2) was achieved using an In Vivo2 hypoxic workstation (Ruskinn, Bridgend, UK).

2. Cell viability assay (MTT assay)

The MTT reagent (3-(4,5-dimethylthiazol-2-yl)-2,5-diphenyltetrazolium bromide) was used to determine cell death as originally described by Mosmann [6] and modified by Cuvillier et al. [7]. Briefly, cells were seeded 5,000 to 10,000 cells/well in 24-well plates depending on the cell type and allowed to attach overnight. All of the complexes were dissolved in DMSO. The concentration of the complexes was calculated according to the elemental composition of the complexes determined by the elemental analyses. Media in the presence of the tested complexes were added and serially diluted to various concentrations (from 5 µM to 0.01 µM). Next to these concentrations, for DHA 50, 20 and 10 µM and for the cationic bisNHC gold(I) complex 3 0.001 µM have been used. The maximum concentration of DMSO in media did not exceed 0.5 % (v/v). After 72 h of treatment, cells were incubated at 37 °C and 5% CO_2 with 25 µL MTT solution (5 mg/mL; Sigma-Aldrich) in 24-well plates for approximately 3 to 4 h. After solubilization with 500 µL of lysis buffer (DMSO), formazan was quantified by spectrophotometry with a microplate reader at 570 nm absorbance. The GI_{50} values corresponding to the concentration that caused 50% inhibition of cell proliferation were calculated from dose-response curves obtained by nonlinear regression analysis (Prism 8.3,

Graphpad Software, San Diego). All the results were calculated from data obtained in three independent experiments.

3. Clonogenic assay

PC-3 and T24 cells were counted and seeded (500 cells/well) to 6-well plates. Cells were allowed to attach overnight and then treated with different concentrations of complex **2a** (0.01 μM，0.1 μM, 0.25 μM, 0.5 μM, 1 μM, 5 μM). After incubation for additional 6 days for T24 and 8 days for PC-3, the cells were washed with PBS (2 mL), fixed with methanol (1 mL) for 20 min and stained with 0.5% crystal violet (2 mL) for 30 min. The relative survival was calculated from the number of single cells that formed colonies of more than 50 cells.

4. Measurement of intracellular reactive oxygen species (ROS)

The cellular ROS generation was shown by the increase of fluorescence intensity of DCF according to a previously reported protocol [8]. Briefly, PC-3, A549, MCF-7 and HepG2 cells were seeded at a density of 50,000 cells/well in 24-well plates for 24 h. Cells were washed with PBS buffer and stained with DCFH-DA (final concentration 20 μM) for 45 min. Then cells were washed with PBS buffer and the culture medium without phenol red containing gold complexes were added to the cells. The fluorescence intensity of DCF (excitation/emission, 485/535 nm) was measured by fluorescence microplate reader at different time points.

5. NRF2 transcriptional activity in MCF-7 and HepG2 cells

The Hep G2 – ARE-LucF, a stable cell line containing a firefly luciferase gene under the control of ARE (BPS Bioscience, Cat # 60513) was primarily used to monitor NRF2 transcriptional activity. Cells were grown at 37°C with 5% CO_2 using MEM medium supplemented with 10% FBS, 1% non-essential amino acids, 1 mM Na-pyruvate, 1% Penicillin/Streptomycin and 600 μg/ml of Geneticin. Cells were harvested from culture in Growth Medium 1K and they were seeded at a concentration of 40,000 cells/well into white clear-bottom 96-well microplate in 45 μL of Growth Medium 1K without Geneticin. Cells were allowed to attach overnight and then treated with different concentrations of complex 2**a** (from 0.01 μM to 20 μM), auranofin (from 0.01 μM to 20 μM) or DHA (from 0.01 μM to 3, 5, 10, 20 and 50 μM), and complex 3 (from 0.01 μM to 20 μM). After incubation at 37 °C and 5% CO_2 for 16 hours, 100 μL ONE-Step luciferase assay reagent (BPS Bioscience Cat # 60690) was

added and rocked at room temperature for over 15 minutes. Then the luminescence of each well was determined by CLARIOstar microplate reader (BMG Labtech, Offenburg, Germany) to quantify induction of ARE. At least three independent experiments were performed as biological triplicates.

The NRF2 Leeporter™ Renilla Reporter – MCF7 cell line (Abeomics, Cat # 14-117ACL) was also used to monitor NRF2 transcriptional activity upon stimulation with tBHQ. Cells were grown at 37°C with 5% CO_2 using Advanced Minimum Essential Medium supplemented with 10% FBS, 2 mM glutamine and 1% Penicillin/Streptomycin, plus 2 µg/ml of Puromycin. Cells were seeded at a concentration of 5,000 cells/well into white clear-bottom 96-well microplate, and allowed to attach overnight. The next day, cells were stimulated with 10 µM tBHQ in presence or not of complex **2a** (from 0.01 µM to 20 µM), auranofin (from 0.01 µM to 20 µM) or DHA (from 0.01 µM to 3, 5, 10, 20 and 50 µM), and complex 3 (from 0.01 µM to 20 µM).

After incubation at 37 °C and 5% CO_2 for 7 hours, cells were washed with 100 µL of DPBS and 20 µL of cell lysate was added to the wells of microplate for 15 min incubation, and then rocked at room temperature for cell lysis to occur. 100 µL of Renilla luciferase assay reagent (Promega, Cat # E2810) per well were added, then the luminescence of each well was determined by CLARIOstar microplate reader (BMG Labtech, Offenburg, Germany) to quantify induction of NRF2.

At least three independent experiments were performed as biological triplicates.

6. NF-κB transcriptional activity

The NF-κB-luciferase – A549 cell line was used for monitoring the activity of NF-κB transcription factor (BPS Bioscience Cat # 60625). The firefly luciferase gene is controlled by 4 copies of NF-κB response element located upstream of the TATA promoter. Cells were grown in DMEM medium supplemented with 10% FBS 1% Penicillin/Streptomycin plus 1 mg/ml of Geneticin. Cells were seeded at a concentration of 10,000 cells/well into white clear-bottom 96-well microplate, and allowed to attach overnight. The next day, cells were stimulated by 1 ng/mL TNFα in presence of not of complex **2a** (from 0.01 µM to 20 µM), auranofin (from 0.01 µM to 20 µM) or DHA (from 0.01 µM to 3, 5, 10, 20 and 50 µM), and complex 3 (from 0.01 µM to 20 µM). After incubation at 37 °C and 5% CO_2 for 7 hours, 100 µL ONE-Step luciferase assay reagent (BPS Bioscience Cat # 60690) was added and rocked at room temperature for

over 15 minutes. Then the luminescence of each well was determined by CLARIOstar microplate reader (BMG Labtech, Offenburg, Germany) to quantify induction of NF-κB.

7. HIF transcriptional activity

HIF Responsive Luciferase Reporter human cervical cancer Hela cell, stably expressing HIF firefly luciferase reporter vector, was used to monitor the activity of HIF transcription factor line (Signosis Cat # SL-0023). Cells were grown in DMEM medium supplemented with 10% FBS 1% Penicillin/Streptomycin plus 100 μg/ml of Hygromycin. Cells were seeded at a concentration of 10,000 cells/well into white clear-bottom 96-well microplate, and allowed to attach overnight. The next day, cells were incubated in hypoxic conditions (0.1% O_2) in presence of not of complex **2a** (from 0.01 μM to 20 μM), auranofin (from 0.01 μM to 20 μM) or DHA (from 0.01 μM to 3, 5, 10, 20 and 50 μM), and complex 3 (from 0.01 μM to 20 μM). After incubation at 37 °C for 7 hours, 100 μL ONE-Step luciferase assay reagent (BPS Bioscience, Cat # 60690) was added and rocked at room temperature for over 15 minutes. Then the luminescence of each well was determined by CLARIOstar microplate reader (BMG Labtech, Offenburg, Germany) to quantify induction of HIF.

8. Isobologram construction

The isobologram analysis evaluates the nature of interaction of two drugs, i.e., drug A (e.g., complex 2a) and drug B (e.g., sorafenib), at a given effect level. The concentrations required to produce the given effect (e.g., Gi_{50}) are determined for drug A ($IC_{x, A}$) and drug B ($IC_{x, B}$) and indicated on the x and y axes of a two-coordinate plot, forming the two points ($IC_{x, A}$, 0) and (0, $IC_{x, B}$). The line connecting these two points is the additivity line. Then, the concentrations of A and B contained in combination that provide the same effect, denoted as ($C_{A, x}$, $C_{B, x}$), are placed in the same plot. Synergy, additivity, or antagonism is indicated when ($C_{A, x}$, $C_{B, x}$) is located below, on, or above the line, respectively.

Combination index (CI) is calculated by the following equation:

$$CI = \frac{C_{A,x}}{IC_{x,A}} + \frac{C_{B,x}}{IC_{x,B}}$$

A CI of less than, equal to, and more than 1 indicates synergy, additivity, and antagonism, respectively.

9. Inhibition of mammalian TrxR

To determine the inhibition of mammalian TrxR, an established microplate reader-based assay was performed with minor modifications [9]. For this purpose, commercially available rat liver TrxR (Sigma-Aldrich, Cat # T9698) was used and diluted with distilled water to achieve 3.5 U/mL. Complex **2a** was freshly dissolved as stock solution in sterile DMSO. 25 µL aliquot of the enzyme and either 25 µL potassium phosphate buffer (pH 7.0) containing complex **2a** in graded concentrations or 25 µL buffer without the complex but DMSO (positive control) were added. The resulting solution (final DMSO concentration of 0.5 % v/v) was incubated at 37 °C for 75 min with moderate shaking in a 96-well plate. To each well, 225 µL of the reaction mixture (1.0 mL reaction mixture consists of 500 µL 100 mM potassium phosphate buffer pH 7.0, 80 µL 100 mM EDTA solution pH 7.5, 20 µL 0.2 % BSA, 100 µL of a 20 mM NADPH and 300 µL distilled water) was added and the reaction was initiated immediately by adding 25 µL of 20 mM DTNB solution. After thorough mixing, the formation of TNB was monitored by a microplate reader at 405 nm at 1 min intervals for 10 measurements. The increase of TNB concentration over time followed a linear tendency ($r^2 \geq 0.99$), and the enzymatic activities were calculated as the slopes (increase in absorbance per second). Non-interference with the assay components was confirmed by a negative control experiment using an enzyme-free test compound. IC_{50} values were calculated as the concentration of the compound decreasing the enzymatic activity of the untreated control by 50%.

References

1. Haynes RK, Chan HW, Cheung MK, Lam WL, Soo MK, Tsang HW*, et al.* C-10 Ester and Ether Derivatives of Dihydroartemisinin−10-α Artesunate, Preparation of Authentic 10-β Artesunate, and of Other Ester and Ether Derivatives Bearing Potential Aromatic Intercalating Groups at C-10. *Eur J Org Chem* 2002(1)**:** 113-132.

2. Sheldrick GM. Phase annealing in SHELX-90: direct methods for larger structures. *Acta Crystallogr Sect A* 1990, **A46**(6)**:** 467-473.

3. Sheldrick GM. Crystal structure refinement with SHELXL. *Acta Crystallogr C Struct Chem* 2015, **71**(Pt 1)**:** 3-8.

4. Legrand O, Simonin G, Perrot JY, Zittoun R, Marie JP. Pgp and MRP activities using calcein-AM are prognostic factors in adult acute myeloid leukemia patients. *Blood* 1998, **91**(12)**:** 4480-4488.

5. Marquardt D, Center MS. Drug transport mechanisms in HL60 cells isolated for resistance to adriamycin: evidence for nuclear drug accumulation and redistribution in resistant cells. *Cancer Res* 1992, **52**(11)**:** 3157-3163.

6. Mosmann T. Rapid colorimetric assay for cellular growth and survival: application to proliferation and cytotoxicity assays. *J Immunol Methods* 1983, **65**(1-2)**:** 55-63.

7. Cuvillier O, Levade T. Sphingosine 1-phosphate antagonizes apoptosis of human leukemia cells by inhibiting release of cytochrome c and Smac/DIABLO from mitochondria. *Blood* 2001, **98**(9)**:** 2828-2836.

8. Zhao Z, Gao P, You Y, Chen T. Cancer-Targeting Functionalization of Selenium-Containing Ruthenium Conjugate with Tumor Microenvironment-Responsive Property to Enhance Theranostic Effects. *Chemistry* 2018, **24**(13)**:** 3289-3298.

9. Rubbiani R, Kitanovic I, Alborzinia H, Can S, Kitanovic A, Onambele LA*, et al.* Benzimidazol-2-ylidene gold(I) complexes are thioredoxin reductase inhibitors with multiple antitumor properties. *J Med Chem* 2010, **53**(24)**:** 8608-8618.

10. ^{1}H and ^{13}C NMR spectra of compounds DHA-C3-C5, 1a-c and 2a-c; ^{1}H-^{1}H COSY, ^{1}H-^{13}C HSQC/HMBC and ^{1}H-^{13}C HMBC spectra of 2a-c.

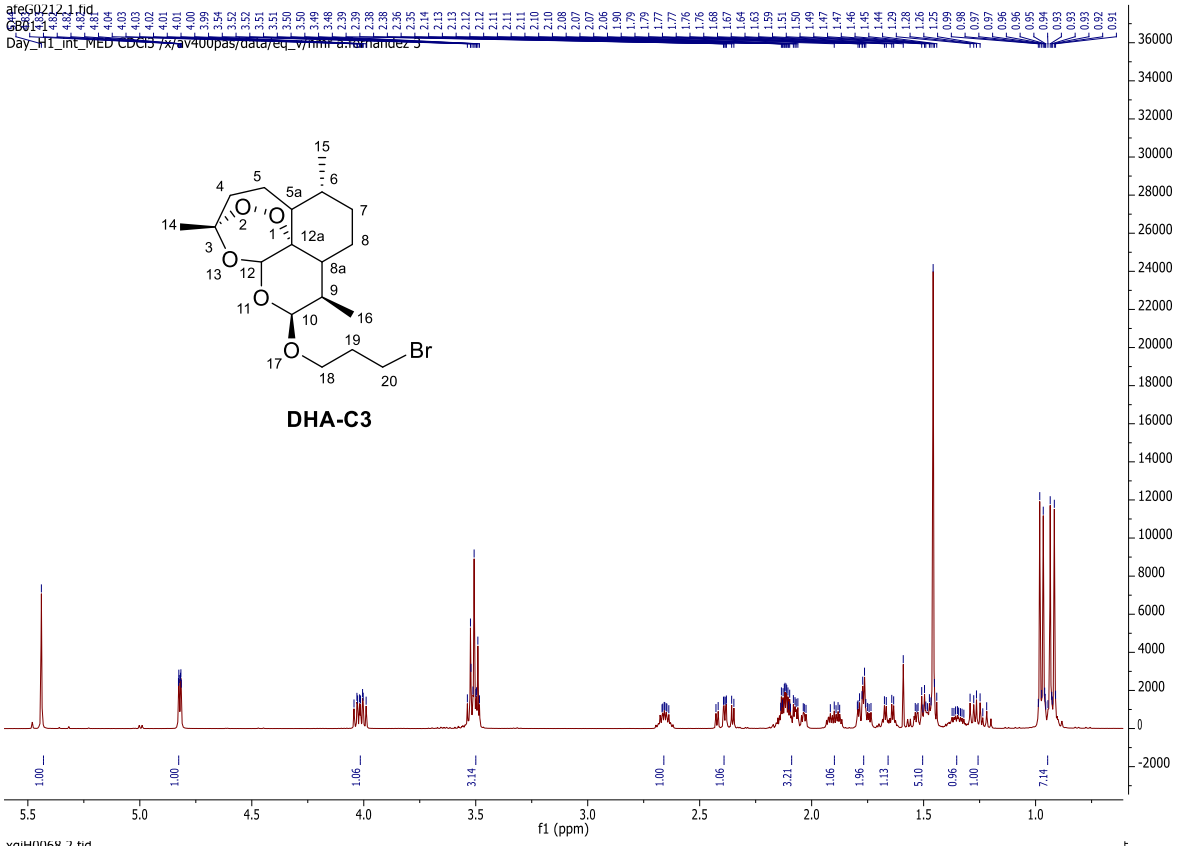

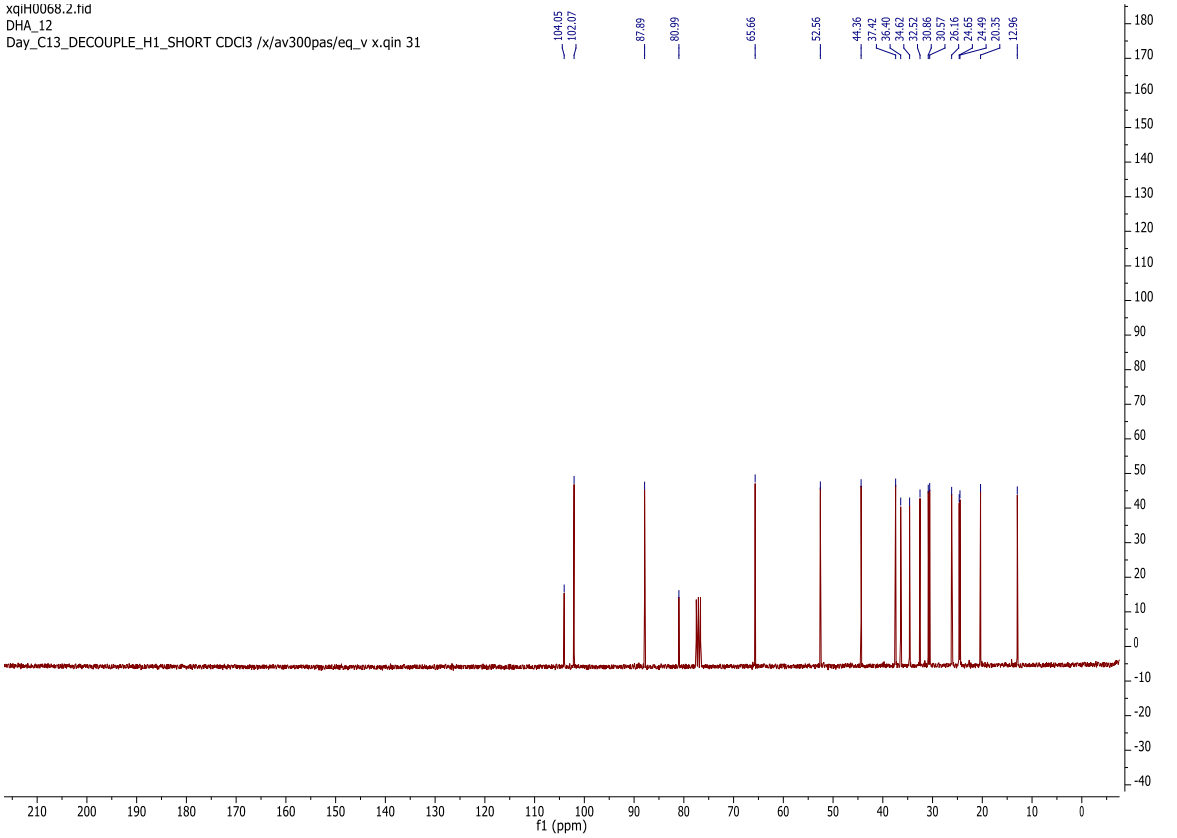

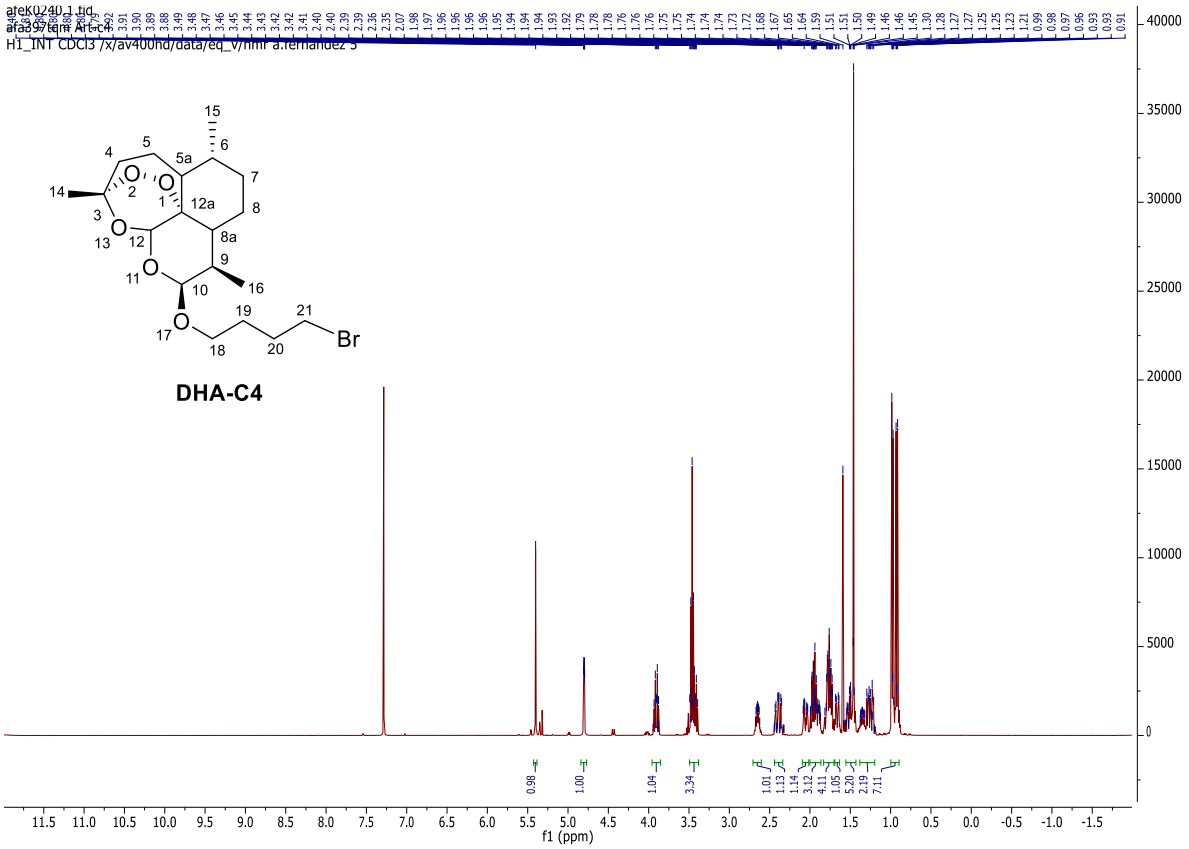
afeK0240.1.fid
afa397tqm Art-c4
H1_INT CDCl3 /x/av400hd/data/eq_v/nmr a.fernandez 5
DHA-C4
f1 (ppm)

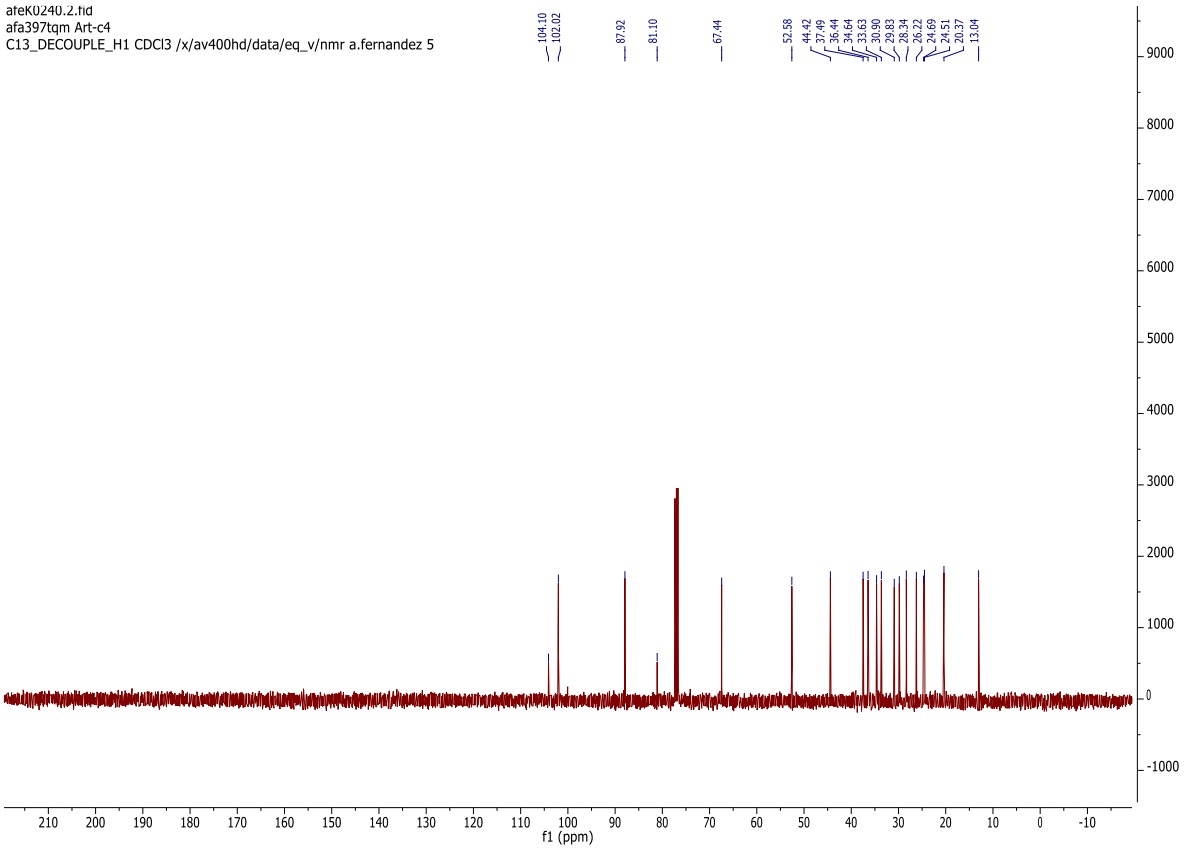
afeK0240.2.fid
afa397tqm Art-c4
C13_DECOUPLE_H1 CDCl3 /x/av400hd/data/eq_v/nmr a.fernandez 5
f1 (ppm)

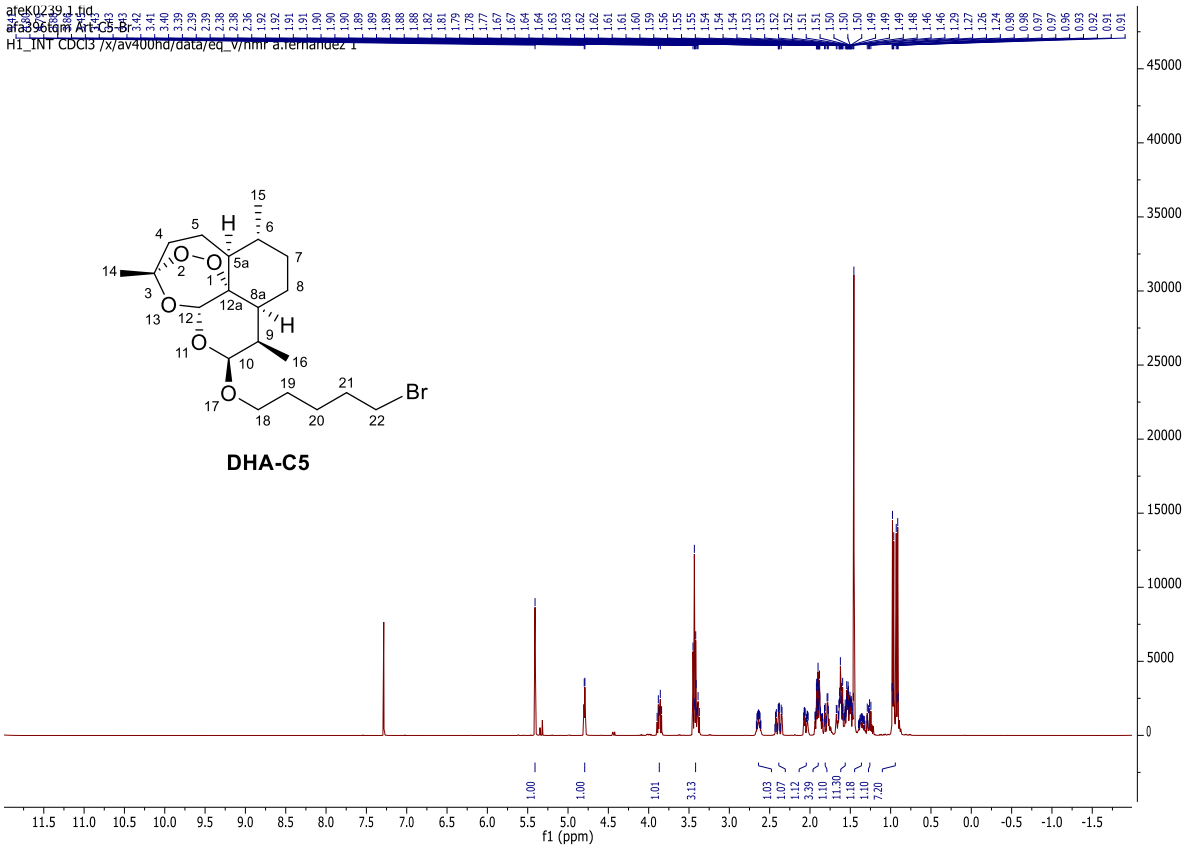
afaK0239_1.fid
afa396tqm Art-C5-Br
H1_INT CDCl3 /x/av400hd/data/eq_v/nmr a.fernandez 1
DHA-C5
f1 (ppm)

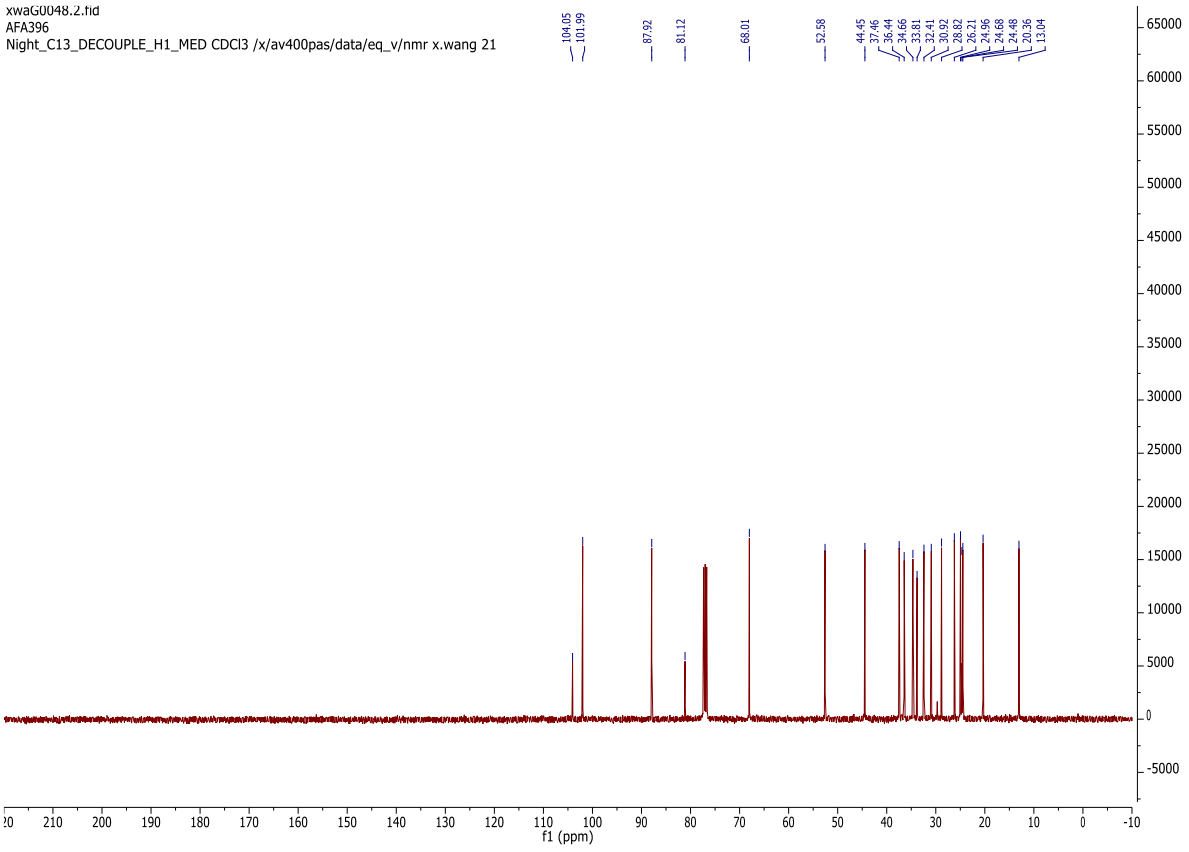
xwaG0048.2.fid
AFA396
Night_C13_DECOUPLE_H1_MED CDCl3 /x/av400pas/data/eq_v/nmr x.wang 21
f1 (ppm)

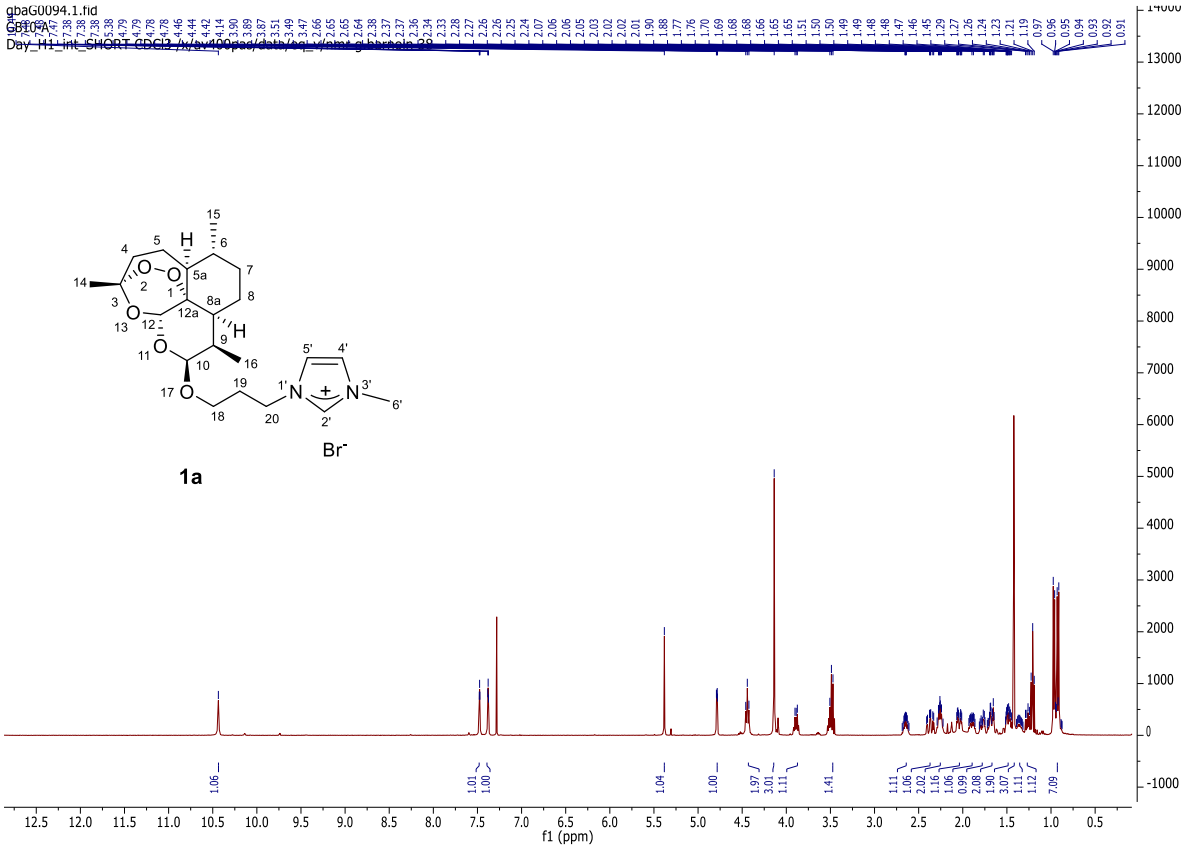
gbaG0094.1.fid
GB10-A
Day_H1_int_SHORT CDCl3 /x/av400pas/data/eq_v/nmr/g.barnole 28
Br-
1a
f1 (ppm)

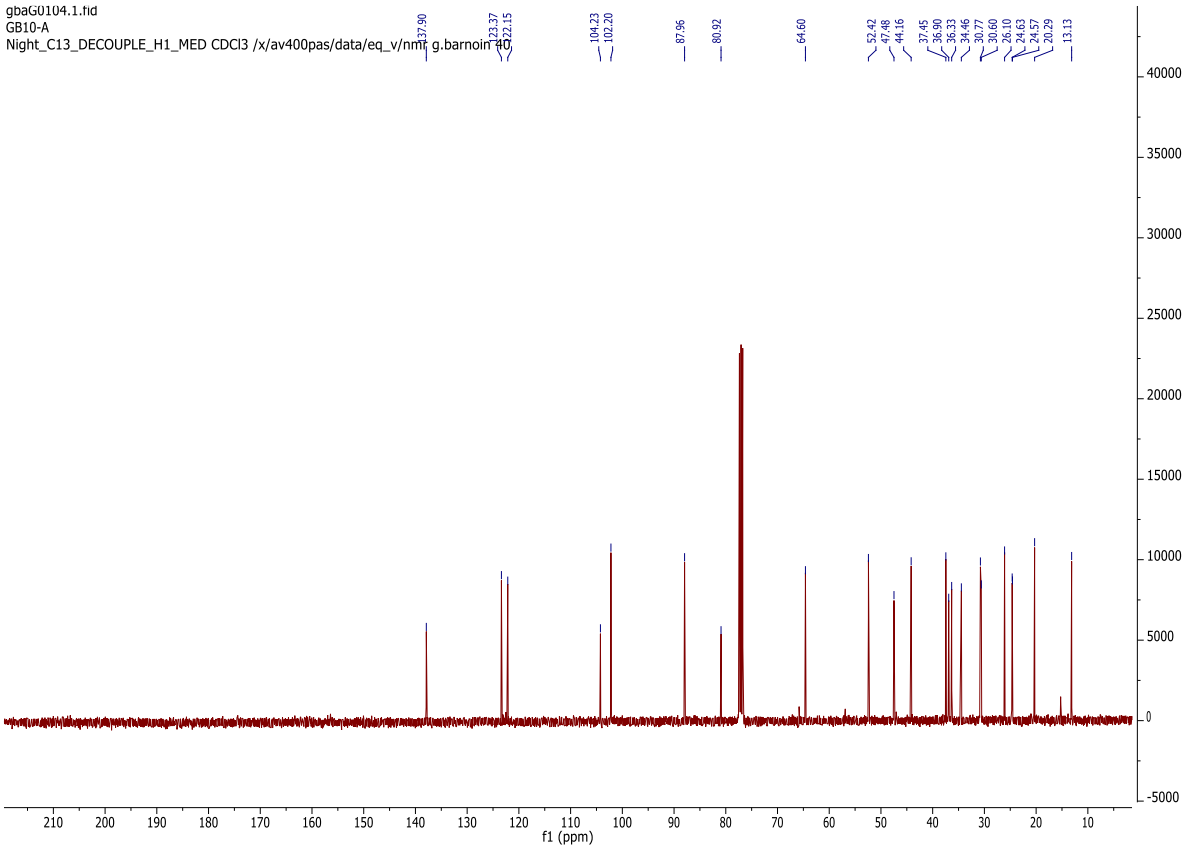
gbaG0104.1.fid
GB10-A
Night_C13_DECOUPLE_H1_MED CDCl3 /x/av400pas/data/eq_v/nmr/ g.barnoin 42
f1 (ppm)

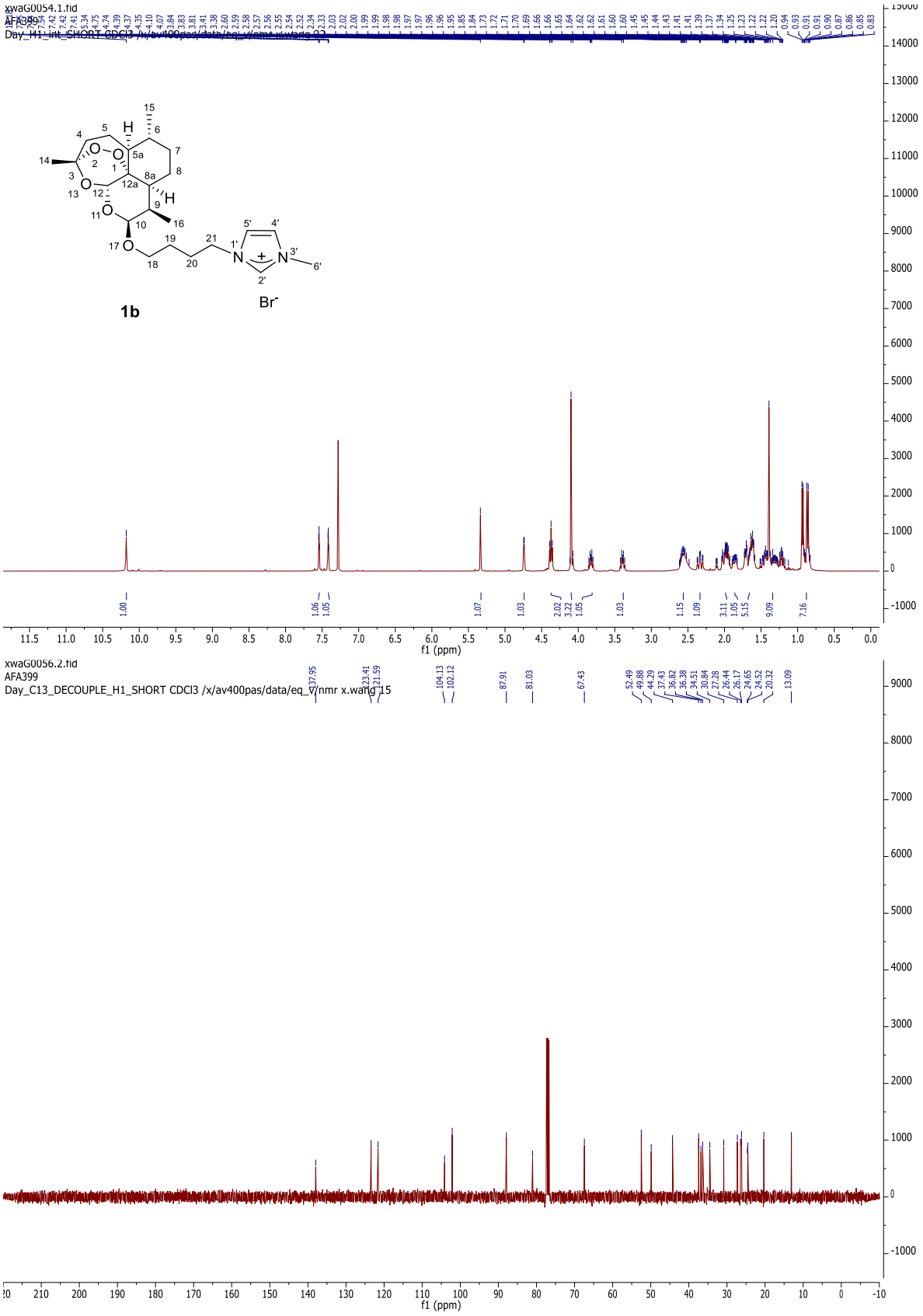
xwaG0054.1.fid
AFA399
Day_H1_int_SHORT CDCl3 /x/av400pas/data/eq_v/nmr x.wang_13
1b
Br-
f1 (ppm)
xwaG0056.2.fid
AFA399
Day_C13_DECOUPLE_H1_SHORT CDCl3 /x/av400pas/data/eq_v/nmr x.wang_15
f1 (ppm)

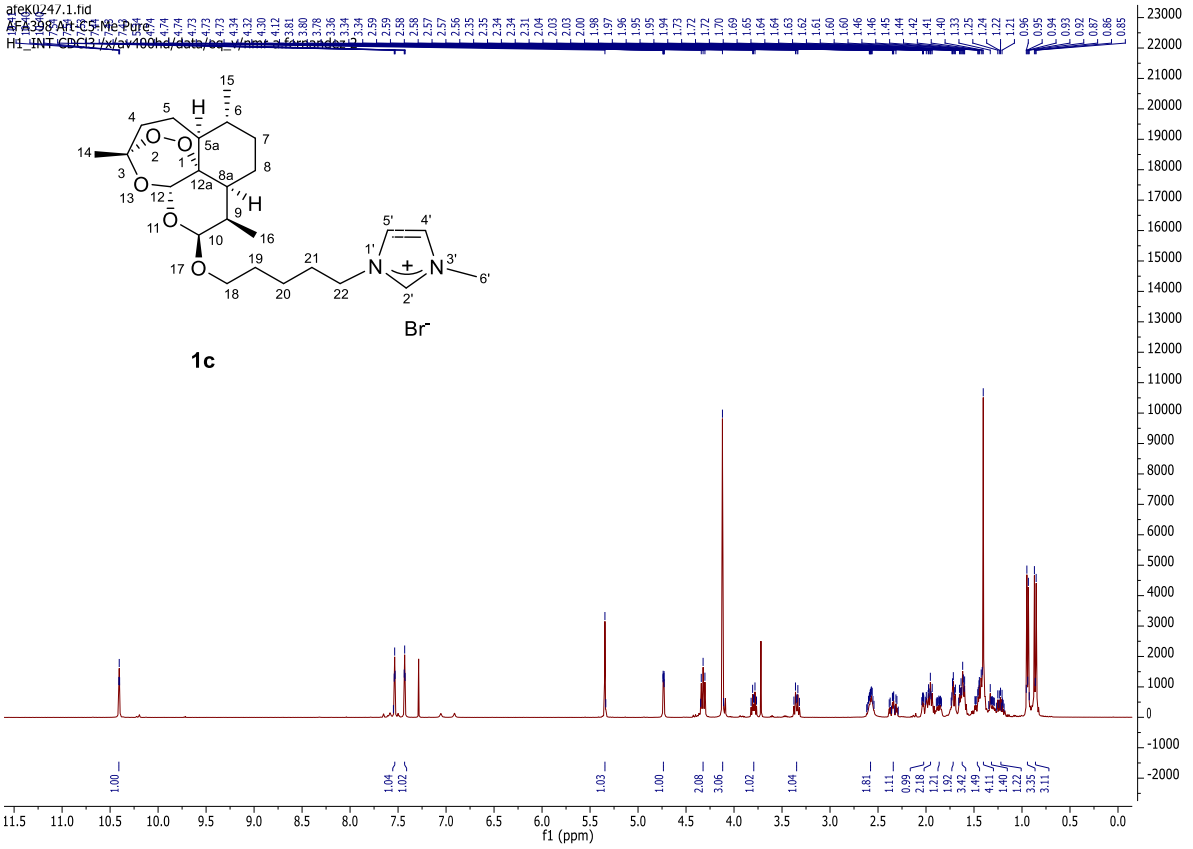
afeK0247.1.fid
AFA398 Art-C5-Me Pure
H1_1NT CDCl3 /x/av400hd/data/eq_v/nmr a.fernandez 2
Br-
f1 (ppm)

1c

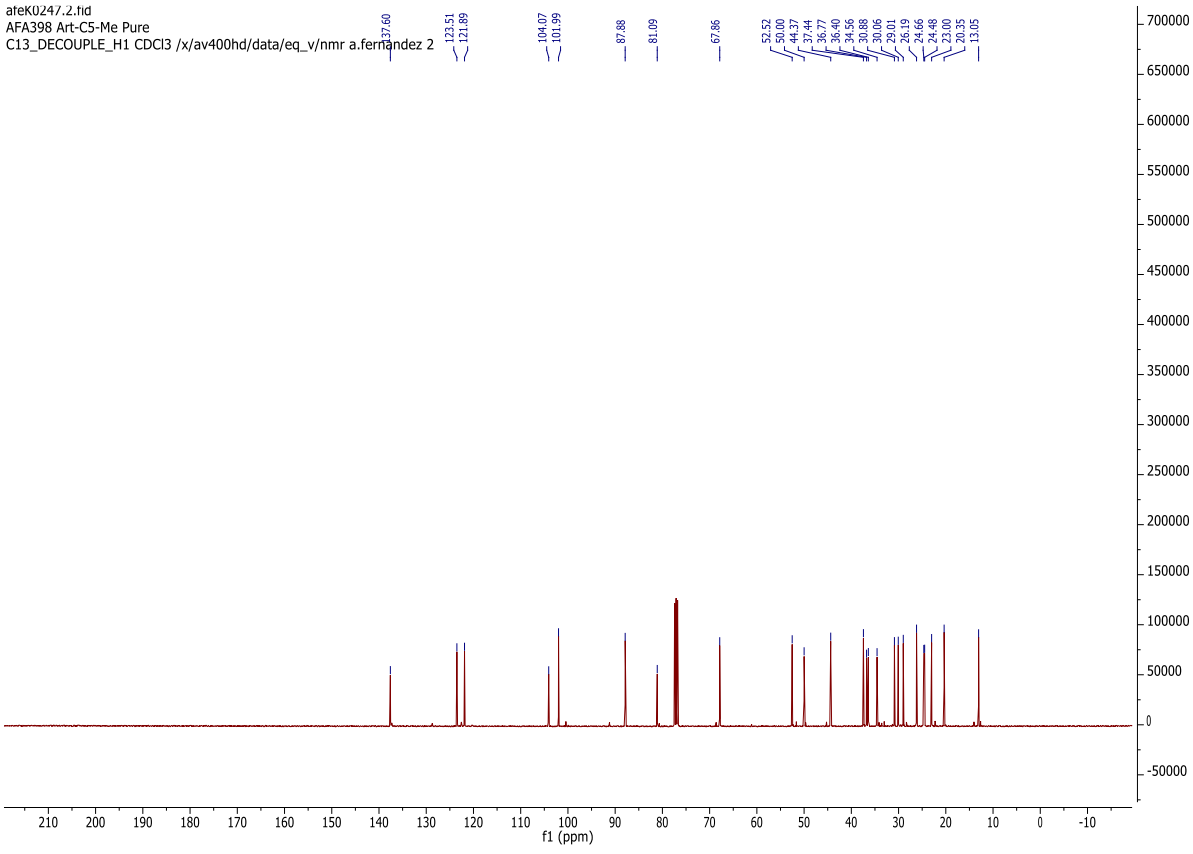
afeK0247.2.fid
AFA398 Art-C5-Me Pure
C13_DECOUPLE_H1 CDCl3 /x/av400hd/data/eq_v/nmr a.fernandez 2
f1 (ppm)

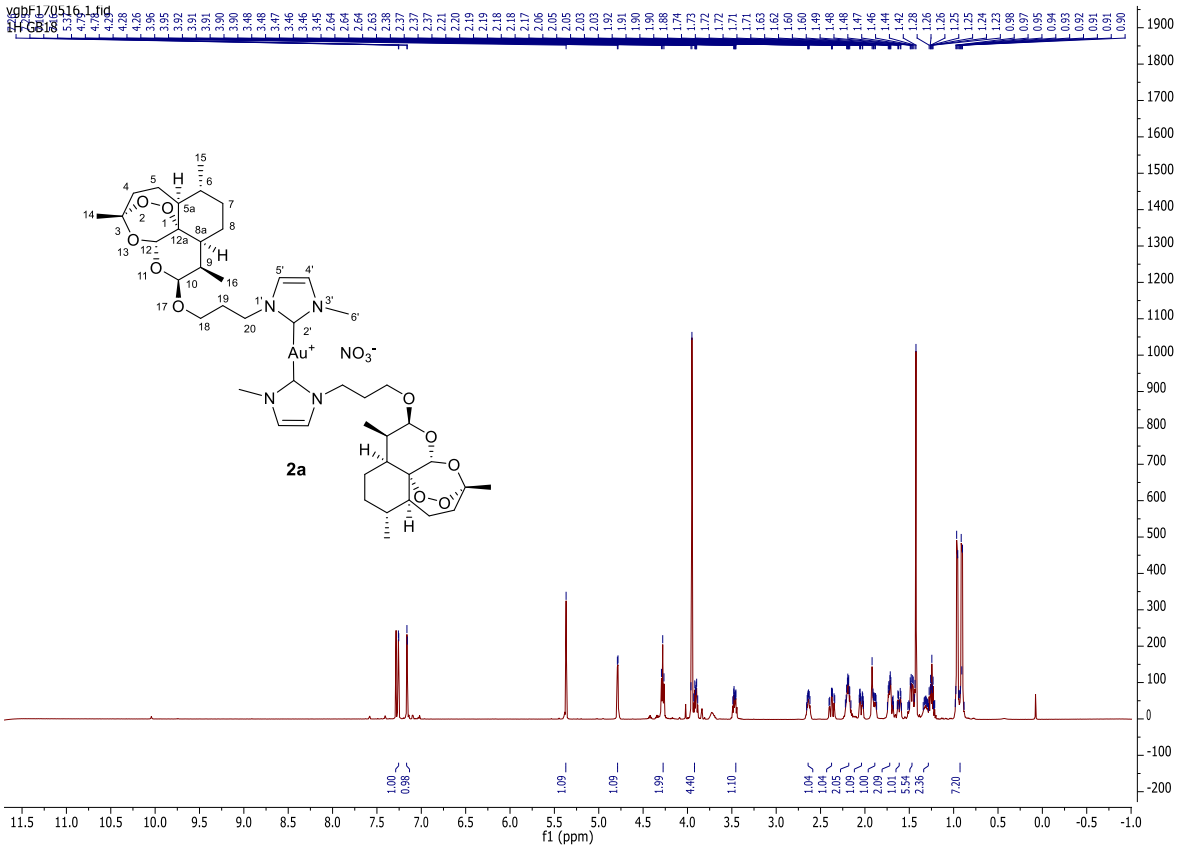
vgbF170516.1.fid
1H GB18
2a
Au+
NO3-
f1 (ppm)

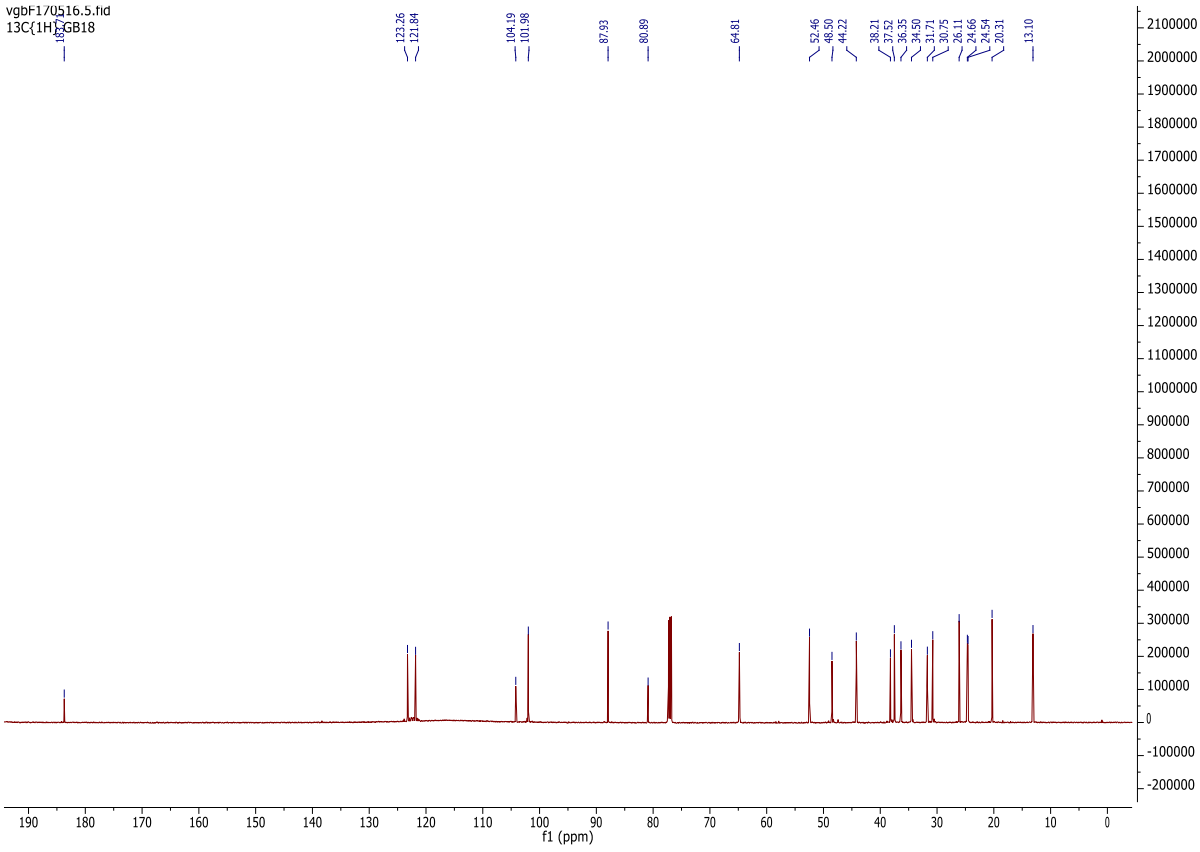
vgbF170516.5.fid
13C{1H} GB18
f1 (ppm)

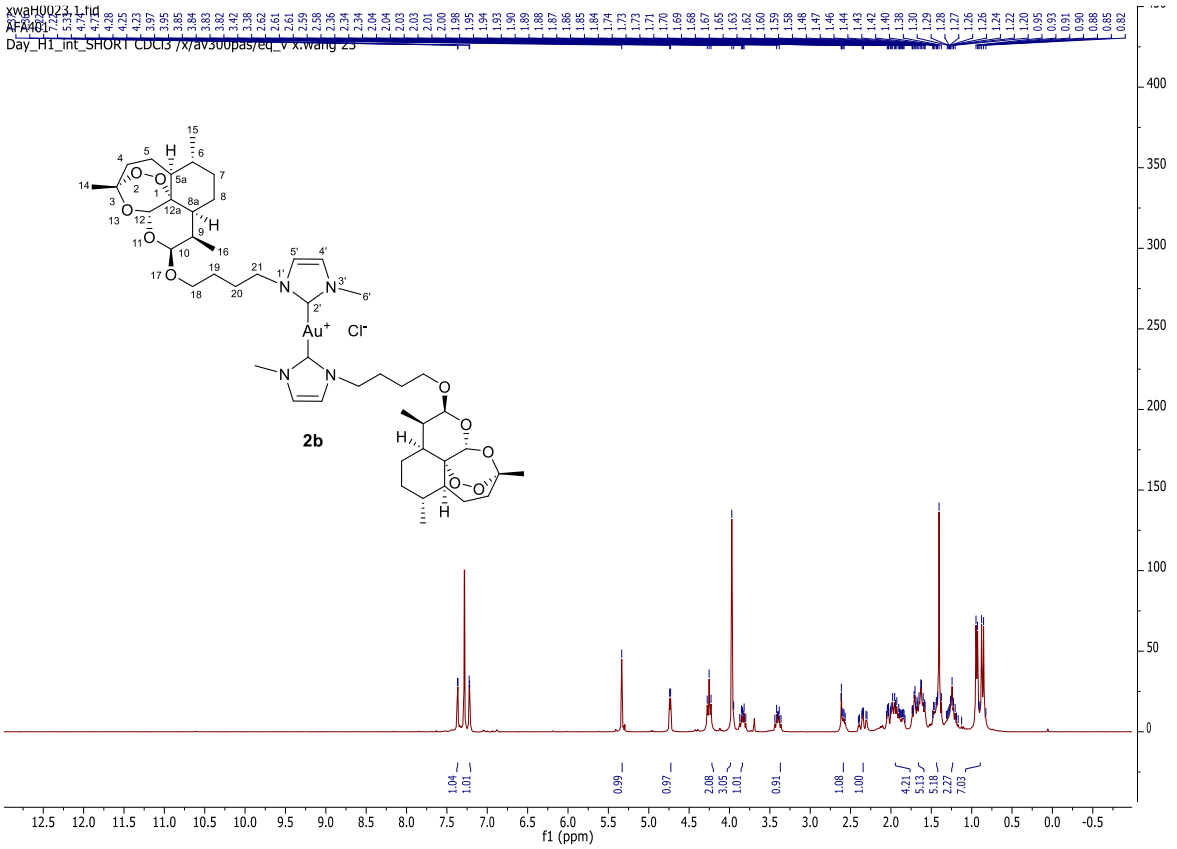
xwaH0023.1.fid
AFA401
Day_H1_int_SHORT CDCl3 /x/av300pas/eq_v x.wang 23
2b
Au+ Cl-
1.04
1.01
0.99
0.97
2.08
3.05
1.01
0.91
1.08
1.00
4.21
5.13
5.18
2.27
7.03
f1 (ppm)

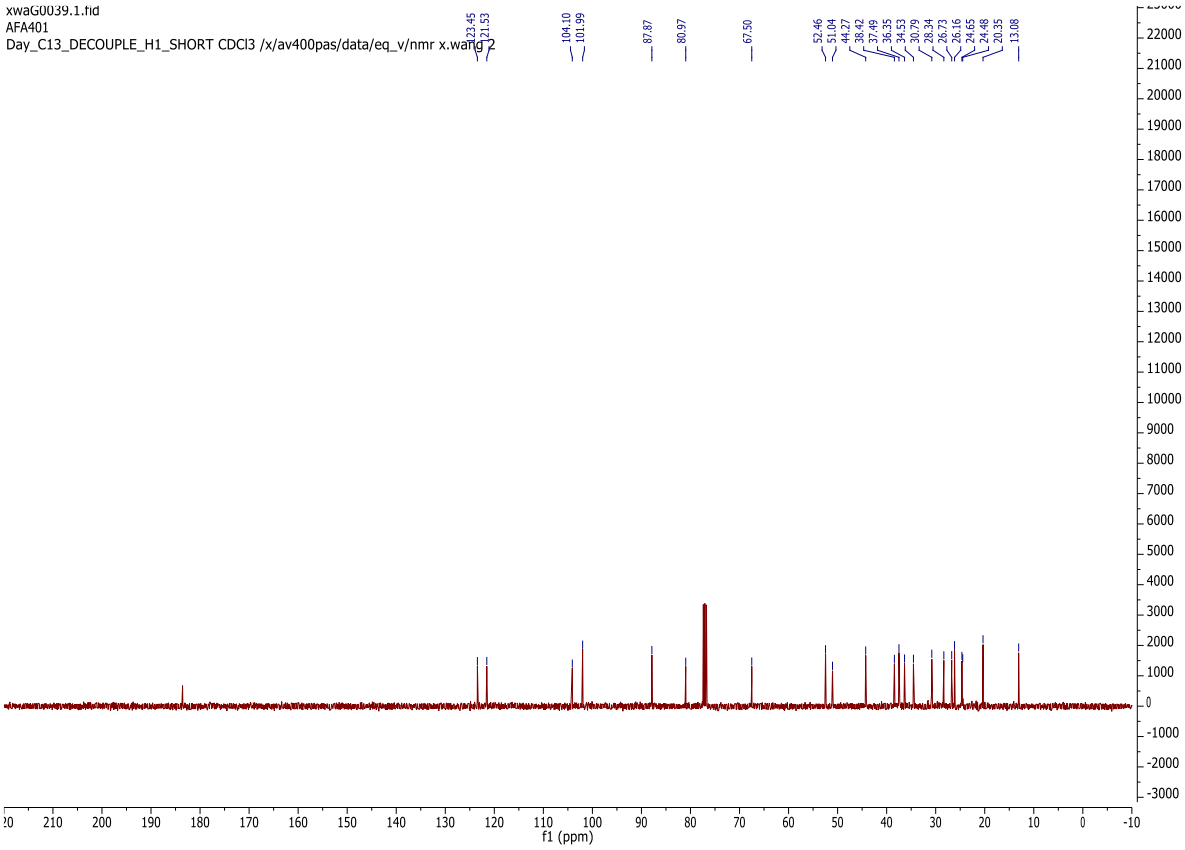
xwaG0039.1.fid
AFA401
Day_C13_DECOUPLE_H1_SHORT CDCl3 /x/av400pas/data/eq_v/nmr x.wang 2
f1 (ppm)

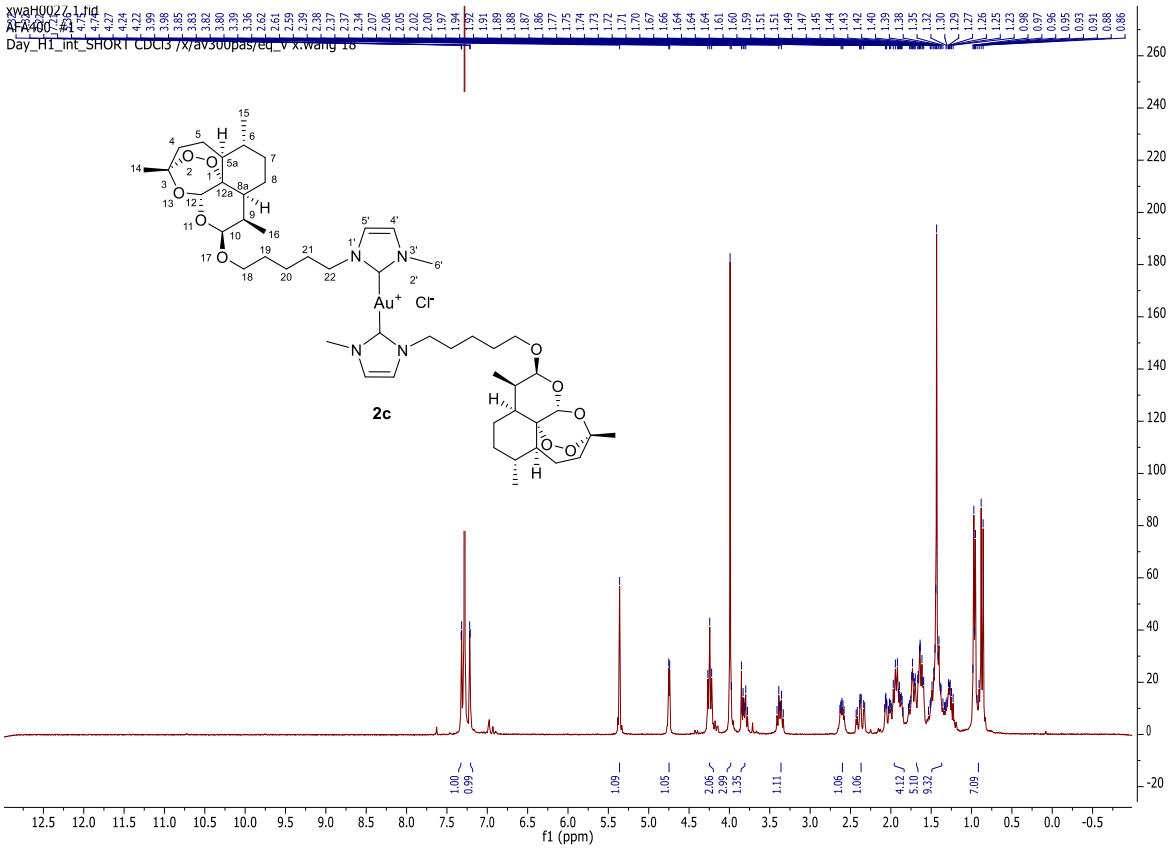
xwaH0027.1.fid
AFA400-#1
Day_H1_int_SHORT CDCl3 /x/av300pas/eq_v x.wang 18
2c
f1 (ppm)

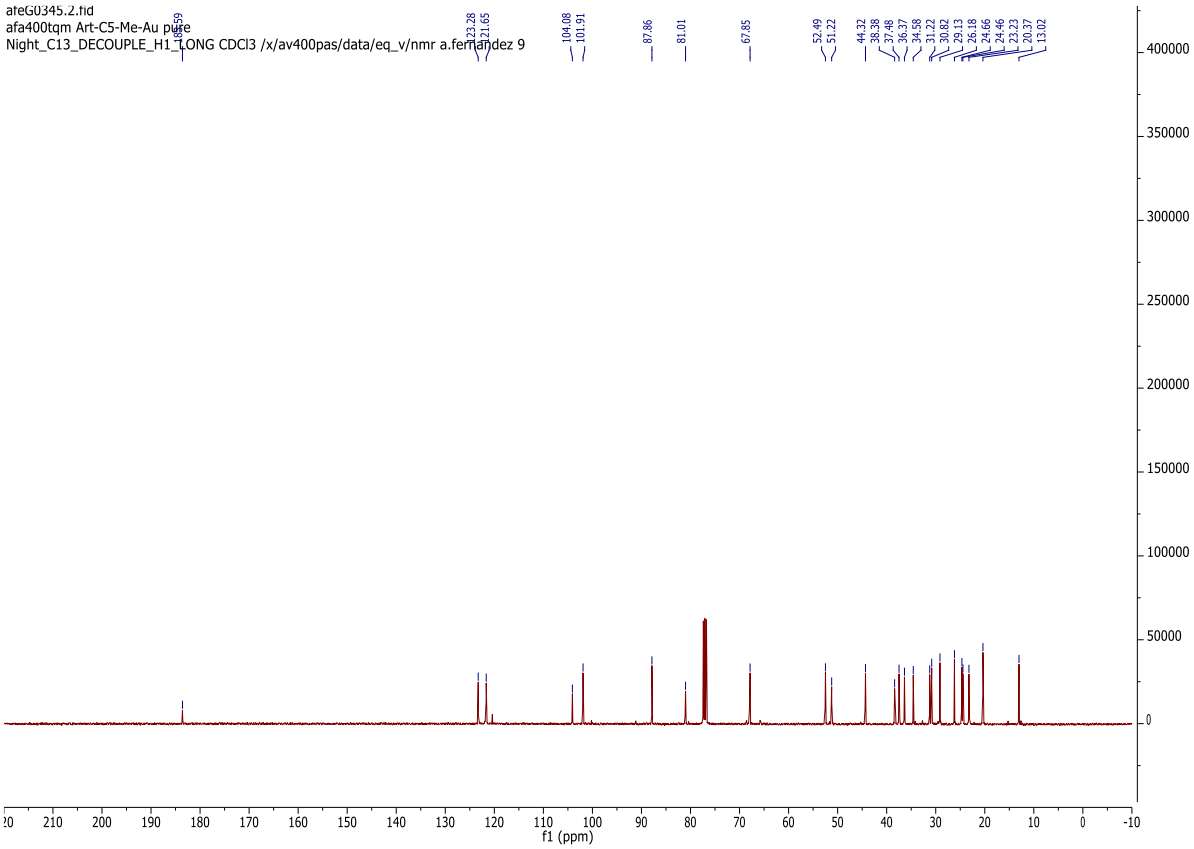
afeG0345.2.fid
afa400tqm Art-C5-Me-Au pure
Night_C13_DECOUPLE_H1_LONG CDCl3 /x/av400pas/data/eq_v/nmr a.fernandez 9
f1 (ppm)

Complex **2a**

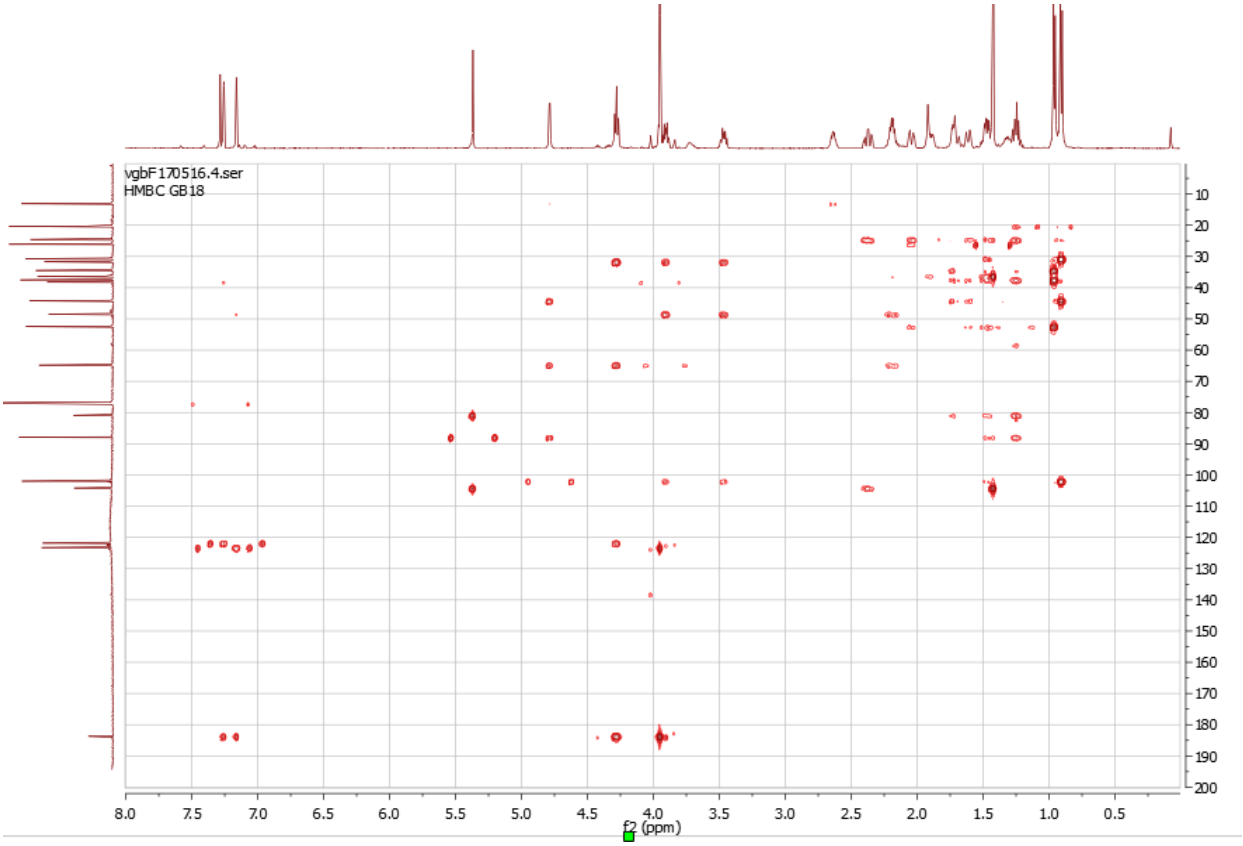
vgbF170516.4.ser
HMBC GB18
f2 (ppm)

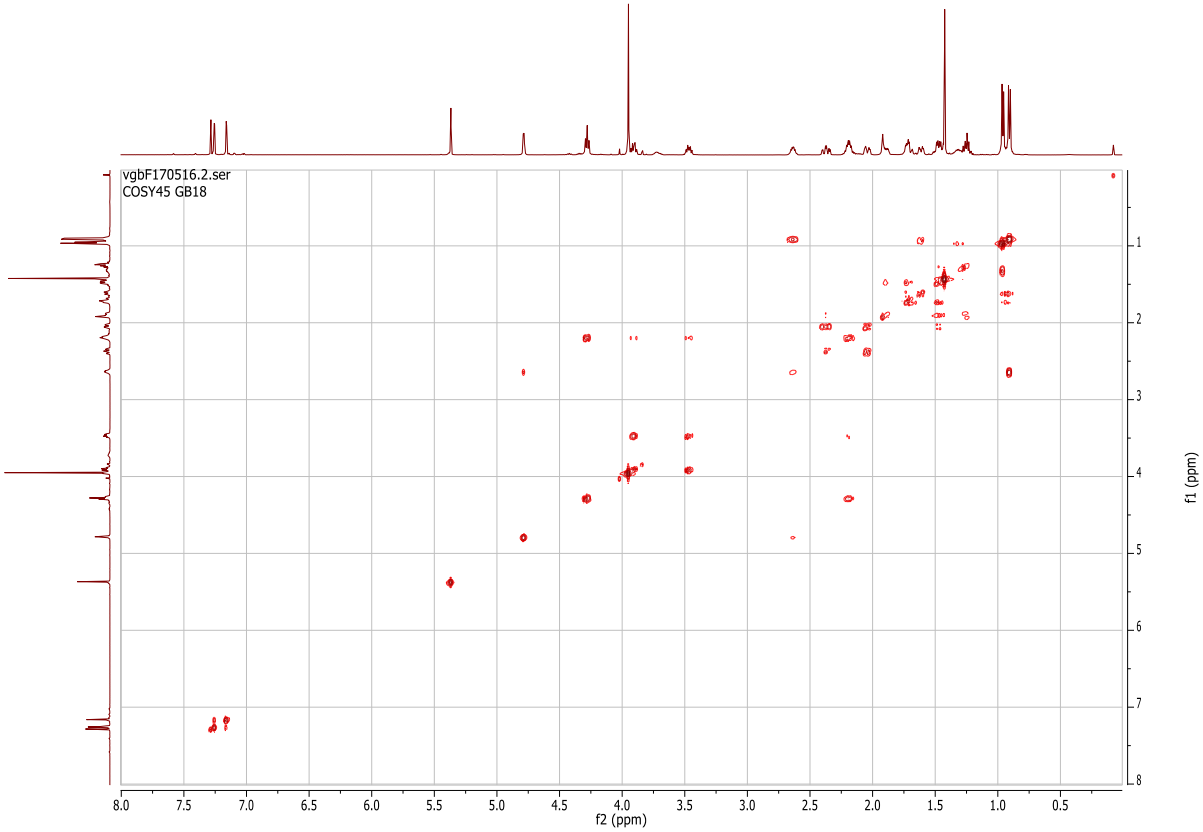
vgbF170516.2.ser
COSY45 GB18
f2 (ppm)
f1 (ppm)

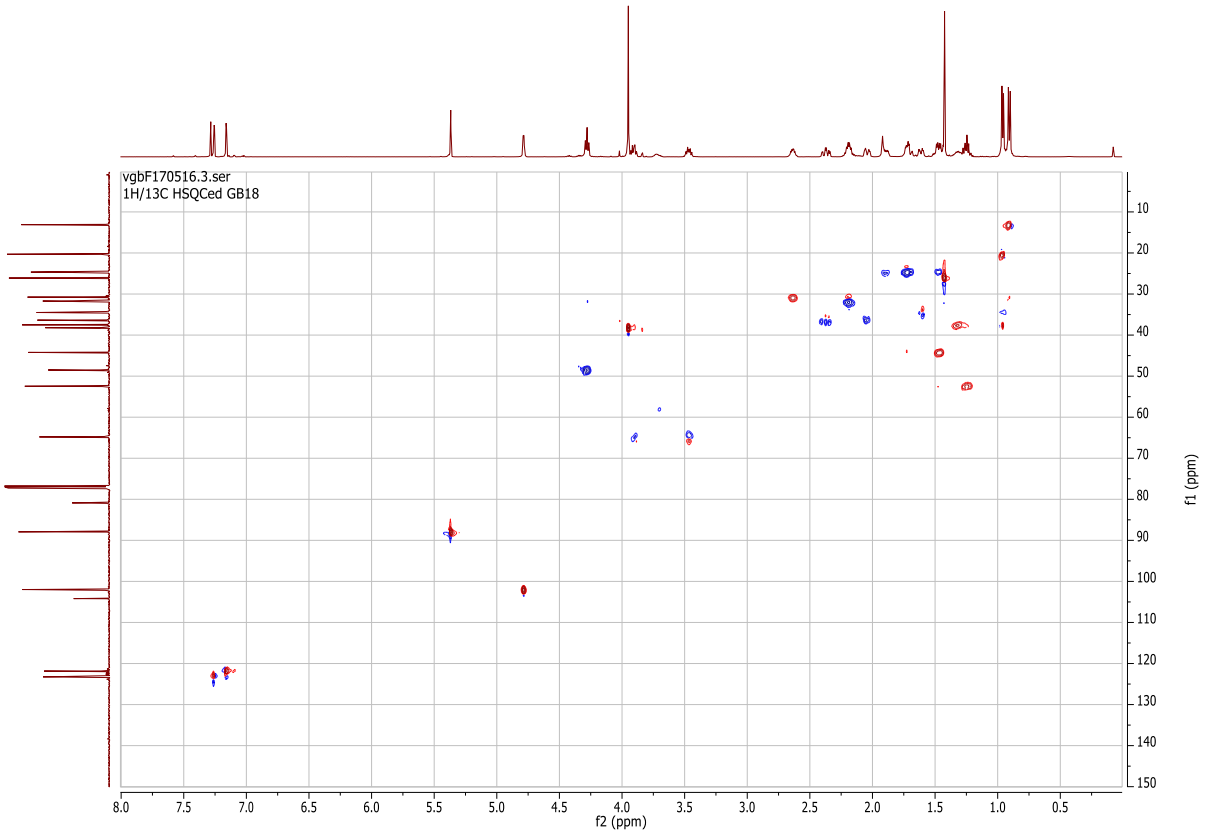
vgbF170516.3.ser
1H/13C HSQCed GB18
f2 (ppm)
f1 (ppm)

Complex **2b**

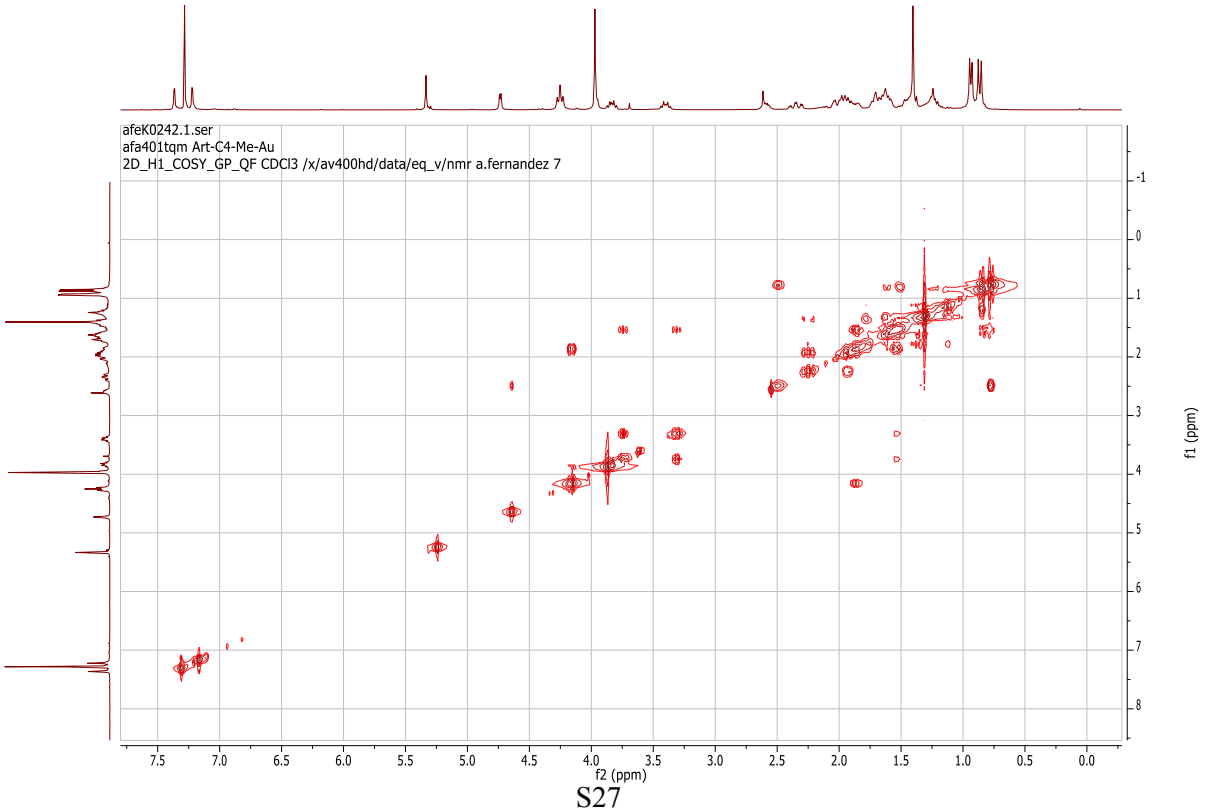
afeK0242.1.ser
afa401tqm Art-C4-Me-Au
2D_H1_COSY_GP_QF CDCl3 /x/av400hd/data/eq_v/nmr a.fernandez 7
f2 (ppm)
f1 (ppm)

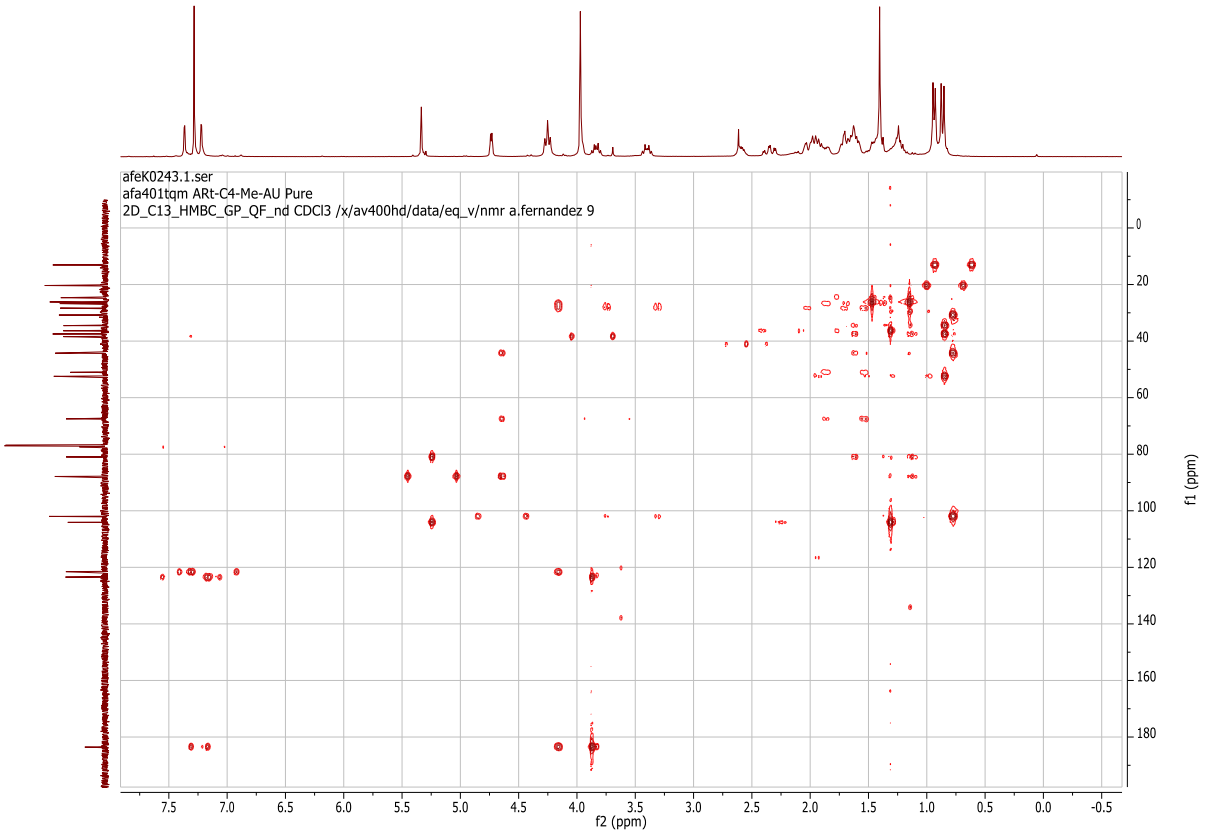
afeK0243.1.ser
afa401tqm ARt-C4-Me-AU Pure
2D_C13_HMBC_GP_QF_nd CDCl3 /x/av400hd/data/eq_v/nmr a.fernandez 9
f2 (ppm)
f1 (ppm)

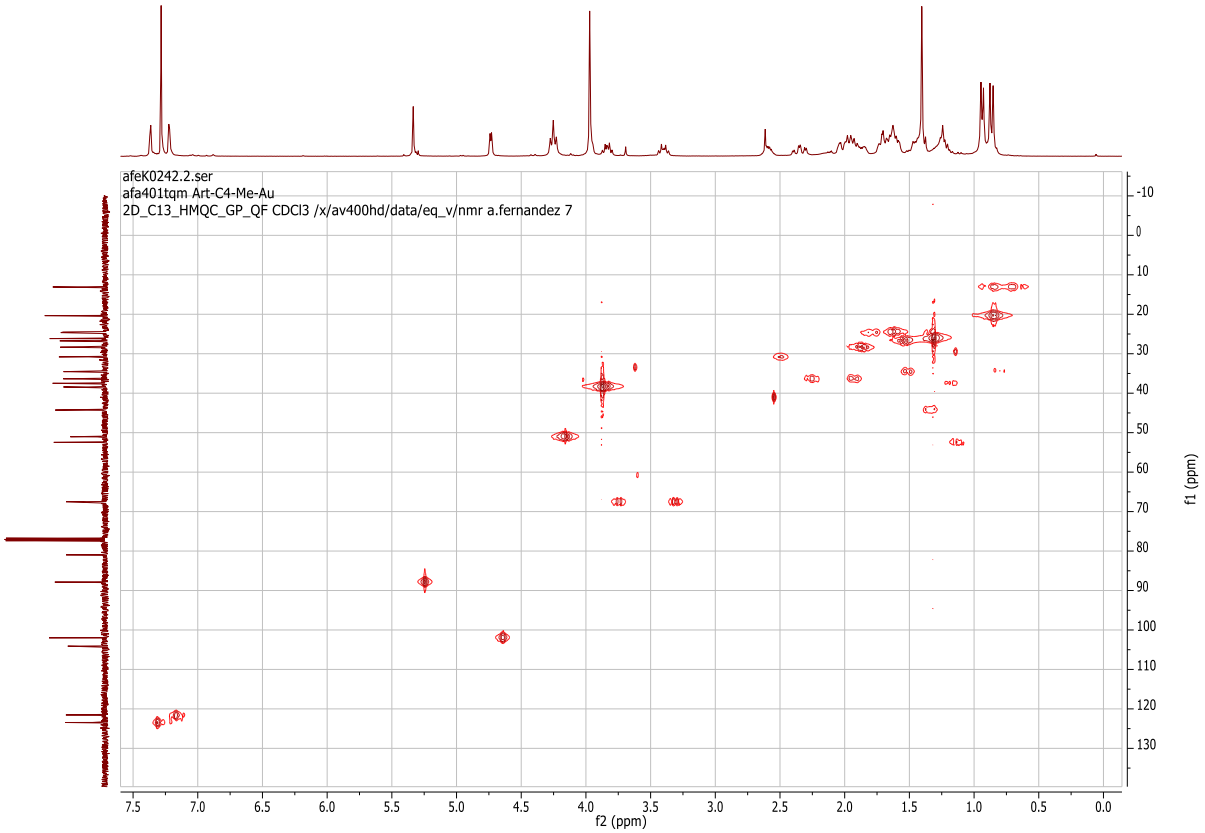
afeK0242.2.ser
afa401tqm Art-C4-Me-Au
2D_C13_HMQC_GP_QF CDCl3 /x/av400hd/data/eq_v/nmr a.fernandez 7
f2 (ppm)
f1 (ppm)

Complex **2c**

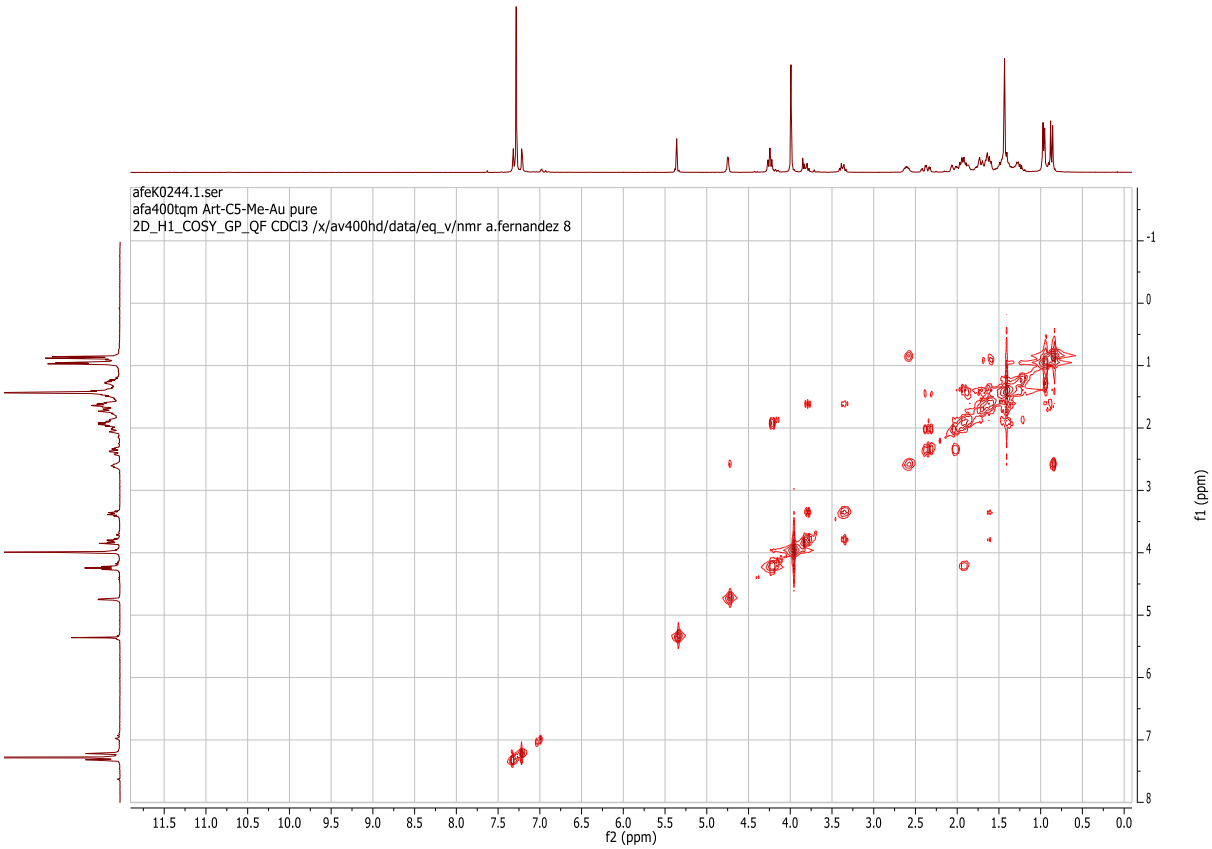
afeK0244.1.ser
afa400tqm Art-C5-Me-Au pure
2D_H1_COSY_GP_QF CDCl3 /x/av400hd/data/eq_v/nmr a.fernandez 8
f2 (ppm)
f1 (ppm)

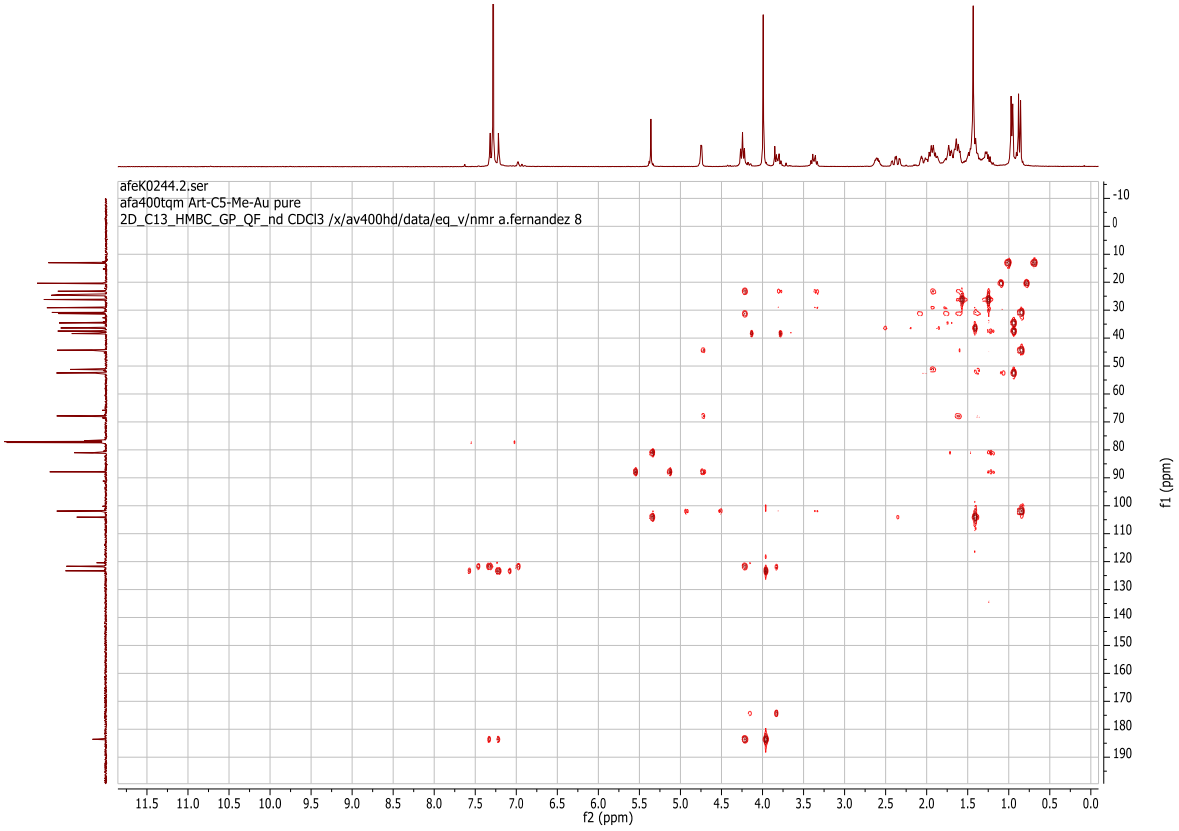
afeK0244.2.ser
afa400tqm Art-C5-Me-Au pure
2D_C13_HMBC_GP_QF_nd CDCl3 /x/av400hd/data/eq_v/nmr a.fernandez 8
f2 (ppm)
f1 (ppm)

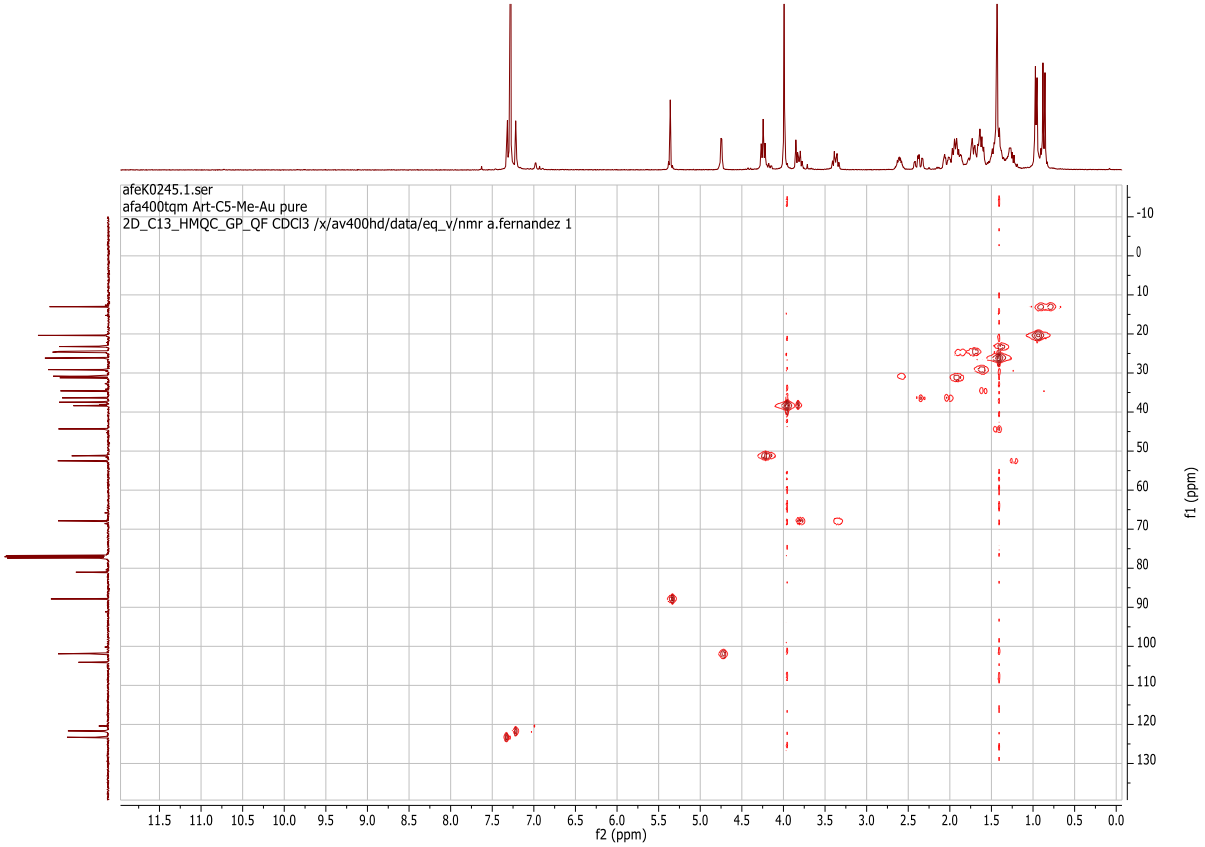
afeK0245.1.ser
afa400tqm Art-C5-Me-Au pure
2D_C13_HMQC_GP_QF CDCl3 /x/av400hd/data/eq_v/nmr a.fernandez 1
f2 (ppm)
f1 (ppm)

Supplementary Figure 1. Colony formation in bladder cancer T24 (top) and prostate cancer PC-3 (bottom) cells treated with increasing concentrations of complex **2a** for 24 h and stained with crystal violet after 1 week of cultivation.

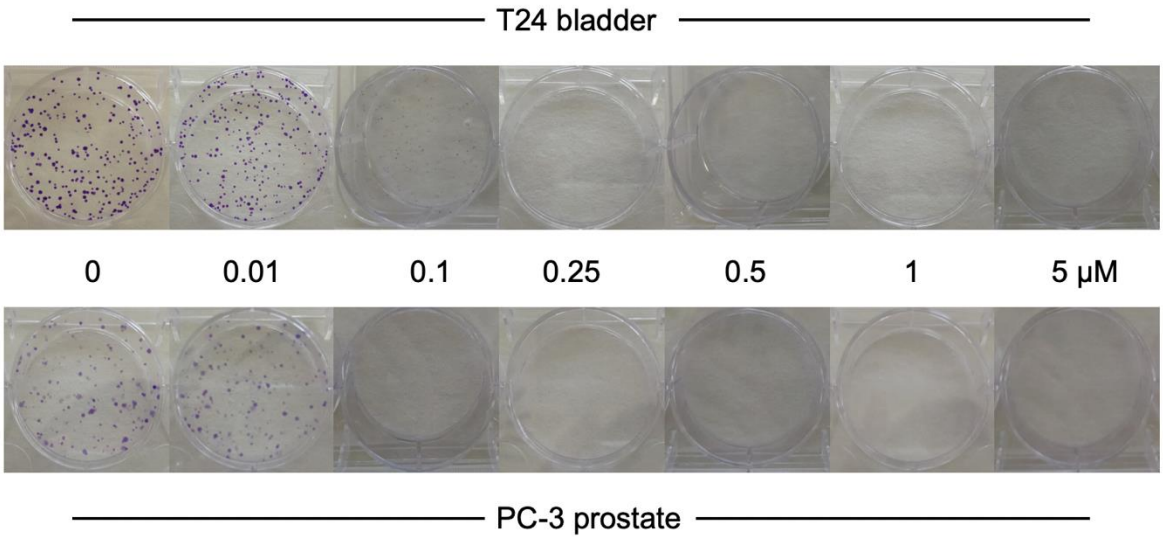

Supplementary Figure 2. ROS generation of DHA, Auranofin and **2a** on a representative panel of cancer cell lineages (DCFH-DA assay).

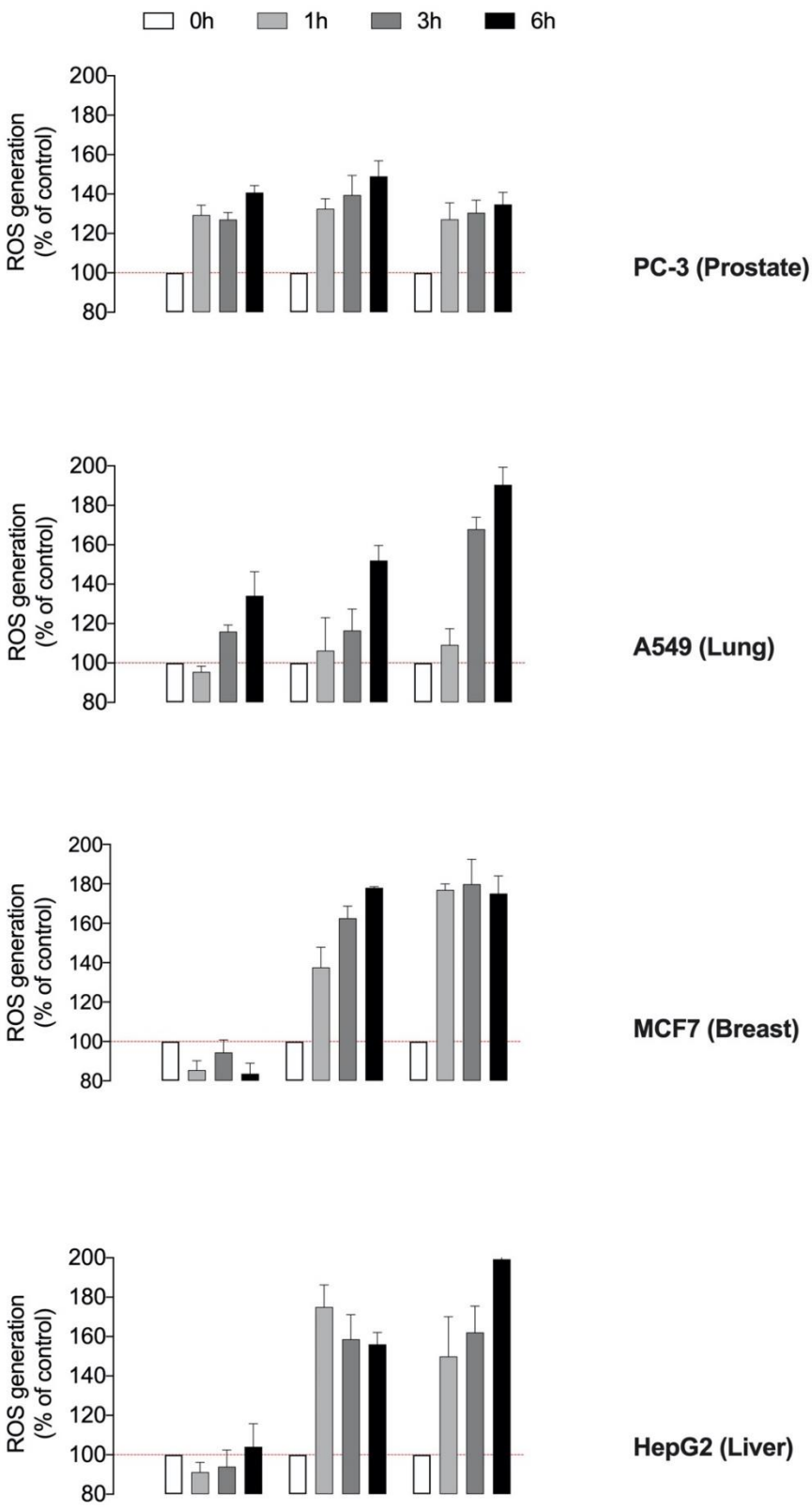

Supplementary Figure 3. Inhibitory effects of Auranofin, DHA, **3** and **2a** compounds on NF-κB and HIF transcriptional activities in A549 and HeLa cancer cell models, respectively.
a, kinetic of NF-κB activation by TNFα in A549 lung cancer cell model in which NF-κB luciferase reporter construct is stably integrated; **b**, the NF-κB inhibitory effect of the described compounds was evaluated in NF-κB/A549 reporter activity in response to 7h of treatment with TNFα; **c**, the HIF inhibitory effect of the described compounds was evaluated in HIF Luciferase Reporter Hela in response to hypoxia (0.1% O_2).

a

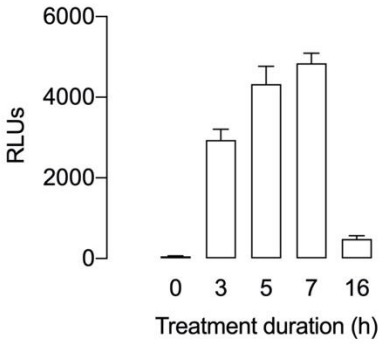

b

Compound	IC_{50} value
Auranofin	2.97 μM
DHA	> 10 μM
3	664 nM

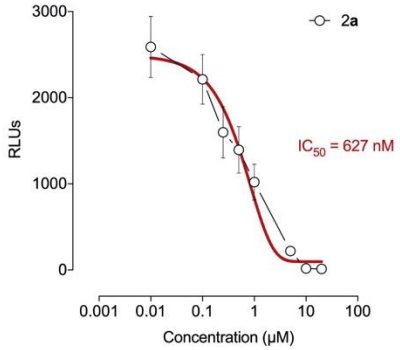

c

Compound	IC_{50} value
Auranofin	745 nM
DHA	> 10 μM
3	2.00 μM

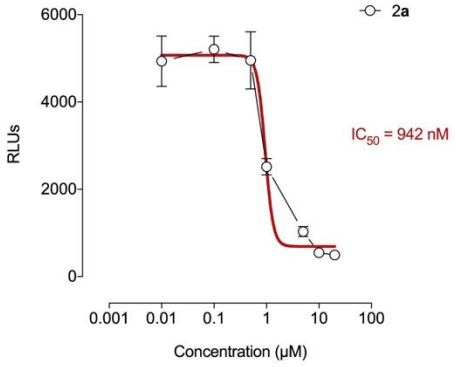

Supplementary Figure 4. IC_{50} value of complex **2a** towards isolated **mammalian** TrxR.